Space Sci Rev (2020) 216:84
https://doi.org/10.1007/s11214-020-00705-7

Comparison of the Deep Atmospheric Dynamics of Jupiter and Saturn in Light of the Juno and Cassini Gravity Measurements

Yohai Kaspi[1] · Eli Galanti[1] · Adam P. Showman[2] · David J. Stevenson[3] · Tristan Guillot[4] · Luciano Iess[5] · Scott J. Bolton[6]

Received: 26 August 2019 / Accepted: 9 June 2020

Abstract The nature and structure of the observed east-west flows on Jupiter and Saturn have been a long-standing mystery in planetary science. This mystery has been recently unraveled by the accurate gravity measurements provided by the Juno mission to Jupiter and the Grand Finale of the Cassini mission to Saturn. These two experiments, which coincidentally happened around the same time, allowed the determination of the overall vertical and meridional profiles of the zonal flows on both planets. This paper reviews the topic of zonal jets on the gas giants in light of the new data from these two experiments. The gravity measurements not only allow the depth of the jets to be constrained, yielding the inference that the jets extend to roughly 3000 and 9000 km below the observed clouds on Jupiter and Saturn, respectively, but also provide insights into the mechanisms controlling these zonal flows. Specifically, for both planets this depth corresponds to the depth where electrical conductivity is within an order of magnitude of 1 $\mathrm{S\,m^{-1}}$, implying that the magnetic field likely plays a key role in damping the zonal flows. An intrinsic characteristic of any gravity inversion, as discussed here, is that the solutions might not be unique. We analyze the robustness

Understanding the Diversity of Planetary Atmospheres
Edited by François Forget, Oleg Korablev, Julia Venturini, Takeshi Imamura, Helmut Lammer and Michel Blanc

Electronic supplementary material The online version of this article (https://doi.org/10.1007/s11214-020-00705-7) contains supplementary material, which is available to authorized users.

✉ Y. Kaspi
yohai.kaspi@weizmann.ac.il

1 Dept. of Earth and Planetary Sciences, Weizmann Institute of Science, Rehovot, 76100, Israel

2 Lunar and Planetary Laboratory, University of Arizona, Tucson, AZ 85721-0092, USA

3 Division of Geological and Planetary Sciences, California Institute of Technology, Pasadena, CA, 91125, USA

4 Université Côte d'Azur, OCA, Lagrange CNRS, 06304 Nice, France

5 Sapienza Universitá di Roma, 00184, Rome, Italy

6 Southwest Research Institute, San Antonio, TX 78238, USA

Published online: 30 June 2020

of the solutions and present several independent lines of evidence supporting the results presented here.

Keywords Jupiter · Saturn · Juno · Cassini · Planetary atmospheres · Gravity science

1 Introduction

The most prominent visual features on Jupiter and Saturn are their east-west bandings, which have been observed since the invention of the first telescopes in the 17th century. These so-called "zones" (bright regions) and "belts" (dark regions) are related to the two gas giants' east-west jet streams. The exact interplay between these zonal flows and the banded structure of the clouds is not completely understood (see recent review by Fletcher et al. 2020a), yet the eastward (westward) jets are typically accompanied by a zone on the equatorward (poleward) side and a belt on the poleward (equatorward) side. Jupiter has about six distinct jets in each hemisphere (Fig. 1), including a wide superrotating eastward jet centered around the equator and narrower jets at higher latitudes. The fastest jet, reaching 140 $\mathrm{m\,s^{-1}}$, is at latitude 23°N, and is not accompanied by a similar jet in the southern hemisphere, creating a hemispheric asymmetry (Fig. 1). On Saturn, the winds are stronger, with a wider equatorial eastward flow (extending to latitude $\sim 30°$) reaching velocities of nearly 400 $\mathrm{m\,s^{-1}}$. Poleward of the equatorial jet, Saturn has 3–4 distinct zonal jets in each hemisphere (Fig. 1). The jet velocities, measured by cloud tracking (e.g., García-Melendo et al. 2011; Tollefson et al. 2017), and typically quoted relative to Jupiter and Saturn's magnetic field rotation, have been overall very consistent since the first spacecraft observations in the 1970s. As Saturn's magnetic field is almost perfectly axisymmetric, this reference frame has a larger uncertainty for Saturn than for Jupiter, although recent measurements and theoretical calculations have limited the rotation period uncertainty to within a few minutes (Anderson and Schubert 2007; Read et al. 2009; Helled et al. 2015; Mankovich et al. 2019).

Prior to the recent Juno and Cassini missions there have been very little data regarding the flows beneath the cloud tops. The only *in-situ* measurements came from the Galileo probe, which descended in 1995 into Jupiter's atmosphere around latitude 6.5°N. The probe found that the zonal wind velocity increased from 80 $\mathrm{m\,s^{-1}}$ at the cloud level, where the probe entered, to ~ 160 $\mathrm{m\,s^{-1}}$ at a depth of 4 bars, below which the zonal velocity remained nearly constant down to 21 bars (130 km below the clouds), where the probe signal was lost (Atkinson et al. 1996). The fact that fast zonal winds extend so deeply indicates that the zonal flow is not restricted to the thin layer within a few scale heights of the cloud level that is subject to absorption of solar radiation, latent-heat release due to condensation of water and other cloud-layer processes. Still, the depth reached by the Galileo probe is only a mere fraction of the planetary radius, and thus the Galileo probe measurements do not provide definitive evidence regarding how deep the zonal flows extend into the planetary abyss. On Saturn, Cassini observations indicate that low-latitude winds seem to be stronger at the 2–3 bar level than at the cloud level (0.5 bar), while the mid-latitude winds seem to be nearly constant or become weaker with depth (Choi et al. 2009; Studwell et al. 2018). By combining data from Saturn's 2010 giant storm and numerical simulations, Sánchez-Lavega et al. (2011) concluded that the zonal jets extend at least to the water-cloud base at pressures of 10–12 bar. Above the main cloud layer, in the upper troposphere and stratosphere, the lack of distinct cloud features makes tracking wind velocities difficult, and the wind shear can only be indirectly inferred based on temperature measurements (Simon-Miller et al. 2006; Fletcher et al. 2007). For both planets, the zonal winds generally appear to decay with

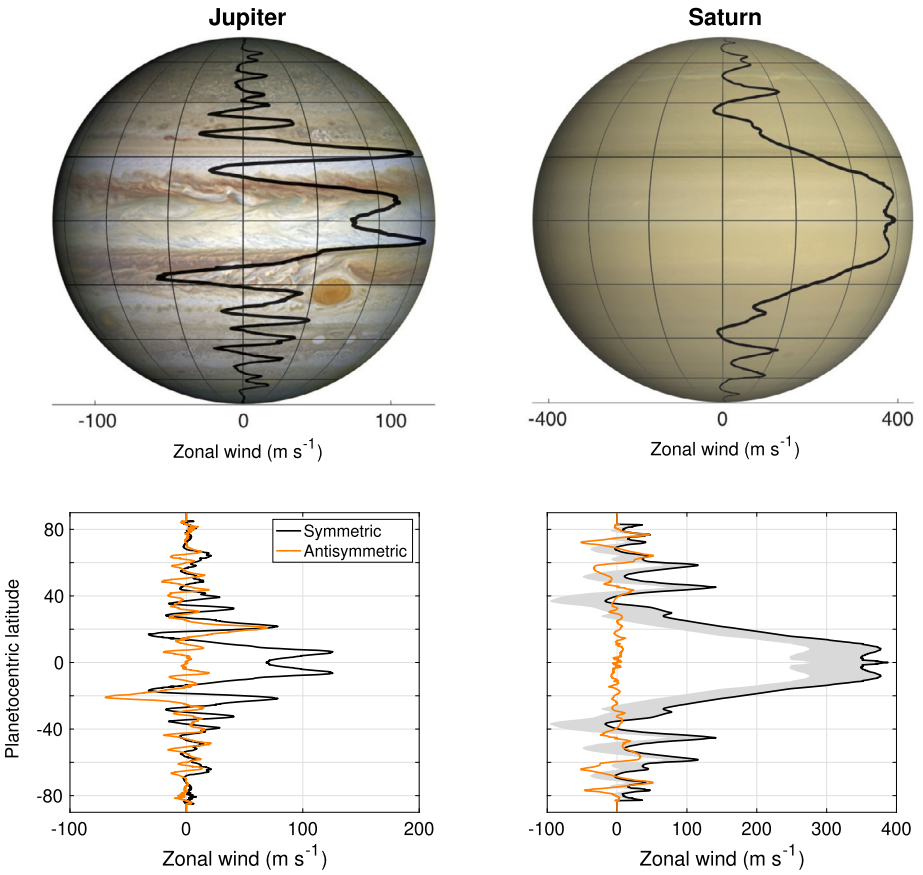

Fig. 1 The zonal wind profile of Jupiter (left) and Saturn (right), divided in the bottom panels into the north-south symmetric (black) and anti-symmetric (orange) parts. In the top panels, the zonal wind profile for Jupiter (Tollefson et al. 2017) is overlaid on an image taken by the Hubble Wide Field Camera in 2014; for the Saturn case, the zonal wind profile (García-Melendo et al. 2011) is overlaid on an image created by Björn Jónsson by combining Cassini and Voyager images and removing the rings. The grid in both images has a 20° latitudinal spread and a 45° longitudinal spread. The scale of the zonal flows for Jupiter is the same as the longitudinal grid on the sphere, and for Saturn it is triple

altitude above the cloud level, although these measurements contain uncertainties as well (Sánchez-Lavega et al. 2019).

The question of how deep the observed jets extend has been debated extensively in the literature since the early observations by the Pioneer and Voyager missions in the 1970s. Two different approaches have been adopted in an effort to explain the jets. According to the first approach, the jets are suggested to be shallow atmospheric features, such as those that appear on terrestrial planets, and thus the dynamics controlling the jets are assumed to be limited to a shallow weather-layer. Geostrophic turbulence theory provides a good understanding of the dynamics controlling jet width and the overall number of jets (Rhines 1975; Held and Larichev 1996; Chemke and Kaspi 2015), and matches the number of jets observed on Jupiter and Saturn. Many shallow-type models have demonstrated the formation of jets similar to those on Jupiter and Saturn, beginning with the models of Williams (1978,

1979), and over the years evolved to more complex models showing formation of multiple jets (e.g., Panetta 1993; Vallis and Maltrud 1993; Cho and Polvani 1996; Huang and Robinson 1998; Lee 2004; Smith 2004; Showman 2007; Kaspi and Flierl 2007; Scott and Polvani 2007; Sayanagi et al. 2008). These shallow-type models typically do not exhibit superrotation, but with particular configurations of bottom drag, internal heating, moist convection or thermal damping they can produce an equatorial superrotating jet and multiple high latitude jets (Scott and Polvani 2008; Lian and Showman 2008, 2010; Liu and Schneider 2010; Warneford and Dellar 2014; Young et al. 2019; Spiga et al. 2020).

The second approach considers deep convection models, in which the source of the jets is suggested to be internal convection columns that interact to form the jets seen at the surface. These ideas also emerged in the 1970s, with the seminal papers of Busse (1970, 1976), and have evolved to more complex interior convention 3D simulations (e.g., Busse 1994; Sun et al. 1993; Christensen 2001; Aurnou and Olson 2001; Wicht et al. 2002; Heimpel et al. 2005; Kaspi et al. 2009; Jones and Kuzanyan 2009; Heimpel et al. 2016; Wicht et al. 2019). These models naturally exhibit superrotation driven by the convergence of convectively driven momentum near the equator, but do not naturally produce the multiple jet structure that appears at higher latitudes. These two approaches have been debated greatly over the past several decades, but due to the lack of observational evidence, the debate has remained unresolved (see reviews by Vasavada and Showman 2005, and Showman et al. 2018). Now, following the Juno and Cassini gravity measurements (Iess et al. 2018, 2019), which are reviewed here, the discussion about the source and structure of the jets can be reinvigorated by these new evidence.

The Juno gravity experiment is one of the key objectives of the Juno mission (Bolton 2005), with the purpose of measuring Jupiter's gravity spectrum to high accuracy, and thereby providing information about Jupiter's interior and atmospheric flows (Hubbard 1999; Kaspi et al. 2010). Juno entered Jupiter's orbit in July 2016, and orbits Jupiter every 53 days. The spacecraft's X- and Ka-band radio links to Earth allow measurements of Jupiter's gravity field via Doppler shifts in the radio frequencies sent to Earth (Bolton et al. 2017; Folkner et al. 2017). The measurements are obtained around the time of the closest approach (perijove), approximately 4000 km above the cloud level (Iess et al. 2018). Throughout the course of the mission, the perijoves are designed to give an overall 360° longitudinal coverage of Jupiter as the perijoves are evenly spaced in longitude (Connerney et al. 2018). In addition, due to the oblateness of Jupiter, the perijoves drift about 1° in latitude poleward every orbit, with the first perijove being at latitude 3°N. As the Juno microwave radiometer and the Ka-band radio experiment cannot operate in tandem, only a subset of the orbits have been devoted to gravity measurements. Nonetheless, the number of gravity orbits to date has sufficed for the error estimate of the measured zonal harmonics to reach saturation (Durante et al. 2020).

Motivated by the Juno mission, the Cassini Grand Finale—the last portion of the Cassini mission before it was terminated by a decent into Saturn—comprised a Juno-like gravity experiment at Saturn. The spacecraft was set into a polar orbit, similar to that of Juno, diving between the planet and the innermost ring, with close, 3500-km, flybys above the cloud level (Edgington and Spilker 2016). Between May and August 2017, Cassini performed 22 such flybys (every six days), out of which, six were devoted to gravity science. As with Jupiter, these gravity measurements have allowed to determine Saturn's gravity spectrum up to J_{10}, and have increased the accuracy of the known harmonics by more than two orders of magnitude (Iess et al. 2019).

In light of these two monumental new measurements, this paper provides a comparative review of what was learned from the gravity measurements regarding the atmospheric

and interior dynamics on Jupiter and Saturn. In Sect. 2, we briefly review the dynamical relations connecting the momentum and gravity fields. In Sect. 3, we review the gravity measurements and compare the measured fields on both Jupiter and Saturn. The interpretation of these results in terms of the resulting vertical and meridional profile of the zonal flows that best match the gravity measurements is presented in Sect. 4. In Sect. 5, we discuss the commonalities between the Juno and Cassini results and their implications for the mechanisms that affect the flow at depth and how the flow might interact with the magnetic field. In Sect. 6, we discuss similar gravity constraints for the zonal flows on Uranus and Neptune, and we conclude in Sect. 7.

2 Theory

The theoretical starting point for understanding the zonal jet dynamics is the Euler equations in the rotating frame

$$(\mathbf{u}\cdot\nabla)\,\mathbf{u}+2\boldsymbol{\Omega}\times\mathbf{u}+\boldsymbol{\Omega}\times(\boldsymbol{\Omega}\times\mathbf{r})=-\frac{1}{\rho}\nabla p+\nabla V, \tag{1}$$

where $\mathbf{u}$ is the 3D velocity vector, ρ is density, p is pressure and V is the body force. The rotation rate of Jupiter is given by the System III rotation (Riddle and Warwick 1976; May et al. 1979), with $\Omega = 1.75\times10^{-4}$ s^{-1}, corresponding to a period of 9.92 hours. For Saturn, there has been significant uncertainty as to its exact rotation rate due to the axisymmetric nature of the planets's magnetic field, but recent studies, using gravity measurements, have constrained the rotation period to 10.57 ± 0.03 hours (Helled et al. 2015; Mankovich et al. 2019). As both giant planets are rapid rotators, for the purpose of studying the large-scale zonal flows, the Rossby number, which is the ratio of the inertial accelerations (first term on lhs in Eq. (1)) to the Coriolis accelerations (second term on lhs in Eq. (1)), is small. In the limit of small Rossby number, the fluid is in geostrophic balance (Pedlosky 1987), meaning:

$$2\boldsymbol{\Omega}\times\rho\mathbf{u}=-\nabla p-\rho\mathbf{g}^{*}, \tag{2}$$

where $\mathbf{g}^{*}$ is the effective gravitational field, $\mathbf{g}^{*}=-\nabla V+\boldsymbol{\Omega}\times(\boldsymbol{\Omega}\times\mathbf{r})$, with the second term being the centrifugal acceleration. Taking the curl of Eq. (2) gives

$$2\boldsymbol{\Omega}\cdot\nabla\,(\rho\mathbf{u})=\nabla\rho\times\mathbf{g}^{*}, \tag{3}$$

where the left-hand side (lhs) has been simplified since the rotation rate vector is constant and using mass conservation, $\nabla\cdot(\rho\mathbf{u})=0$. The rotation rate being constant also implies that $\mathbf{g}^{*}$ can be expressed as a scalar potential, meaning that $\nabla\times\mathbf{g}^{*}=0$, which has been used for the rhs of Eq. (3). This thermal-wind-like relation (Kaspi et al. 2009) is different from the standard thermal-wind used in atmospheric science for a shallow atmosphere (e.g., Vallis 2017) in that the derivatives on the lhs are in the direction of the spin axis and not in the radial direction[1] (an approximation that holds when the planetary aspect ratio between the vertical and horizontal scales is small), and the rhs involves the full density and effective gravity.[2] Thus, this is a general expression applicable to a rotating atmosphere at any depth as long as the Rossby number and friction are small.

[1] Note that $2\boldsymbol{\Omega}\cdot\nabla=2\boldsymbol{\Omega}\frac{\partial}{\partial z}$, where z is the direction parallel to the spin vector ($\boldsymbol{\Omega}$).

[2] Note that the barotropic limit is not simply when the rhs of Eq. (3) vanishes, but rather when the lhs changes as well, resulting in $2\boldsymbol{\Omega}\cdot\nabla\mathbf{u}-2\boldsymbol{\Omega}\nabla\cdot\mathbf{u}=0$. See full derivation in Kaspi et al. (2016).

A considerable simplification to this equation can be taken by assuming sphericity. Without this assumption, the rhs of Eq. (3) will involve several terms coming from the centrifugal terms (Cao and Stevenson 2017a) and the deviation of gravity from radial symmetry, both due to the planetary oblateness and dynamical contributions to the gravity vector (see Eq. (7)). In Galanti et al. (2017) and Kaspi et al. (2018), a careful treatment of all these terms was taken, showing that to leading order, Eq. (3) is given by

$$2\boldsymbol{\Omega}\cdot\nabla\left(\rho_s\mathbf{u}\right)=\nabla\rho'\times\mathbf{g_s}, \tag{4}$$

where ρ has been split into static $\rho_s\left(r\right)$ and dynamical $\rho'\left(r,\theta\right)$ components, r is the radial direction and θ is latitude. Here, $\mathbf{g_s}$ is the radial gravitational acceleration coming from integrating ρ_s. It is important to note that if the spherical assumption is not taken in Eq. (3), the rhs decomposes into several different terms of equal magnitude (Galanti et al. 2017), and using only part of them (Zhang et al. 2015) leads to an inconsistent expansion (see more details below). Since the flows on the giant planets are predominantly in the zonal direction, taking the zonal component of Eq. (4) allows the flow-induced meridional density gradient to be integrated to give the dynamical contribution to the gravity harmonics, given by

$$\Delta J_n=-\frac{2\pi}{Ma^n}\int_{-1}^{1}d\mu\int_{0}^{a}r^{n+2}P_n\left(\mu\right)\rho'\left(r,\mu\right)dr, \tag{5}$$

where M is the planetary mass, a is the planetary mean radius, P_n are the associated Legendre polynomials and $\mu=\sin\left(\theta\right)$. Note that when integrating $\frac{\partial\rho'}{\partial\theta}$ from the zonal component of Eq. (4), for use in Eq. (5), an undetermined radially dependent integration function arises $\left(\rho_0'\left(r\right)\right)$. However, such a function will not project onto the gravity harmonics when multiplied by the P_n in Eq. (5), since

$$\int_{-1}^{1}d\mu\int_{0}^{a}r^{n+2}P_n\left(\mu\right)\rho_0'\left(r\right)dr=0, \tag{6}$$

because the latitudinally dependent associated Legendre polynomials, P_n, have a zero mean. Therefore, in spherical geometry, the dynamical gravity anomalies can be uniquely determined, despite the density anomaly itself being determined only up to an unknown constant of integration (Kaspi et al. 2016).

There has been debate in the literature whether an additional term, namely, $\nabla\rho_s\times\mathbf{g}'$, which appears to be of the same order as the rhs of Eq. (4), should be included in that equation (termed the thermal-gravity wind equation by Zhang et al. 2015). However, this additional term contains a deviation from radial symmetry and therefore it was dropped in going from Eq. (3) to Eq. (4). If this term is retained, then for consistency, other terms from Eq. (3) that involve deviation from radial symmetry, and are of the same order, must be retained as well (Galanti et al. 2017). Then the azimuthal component of Eq. (3) will take the form:

$$\begin{aligned}2\Omega\frac{\partial}{\partial z}\left(\rho_s u\right)=&\frac{g_s^{(r)}}{r}\frac{\partial\rho'}{\partial\theta}-g_s^{(\theta)}\frac{\partial\rho'}{\partial r}+\frac{g'^{(r)}}{r}\frac{\partial\rho_s}{\partial\theta}-g'^{(\theta)}\frac{\partial\rho_s}{\partial r}\\&+\Omega^2\left[\frac{\partial\rho'}{\partial\theta}\cos^2\theta+\frac{\partial\rho'}{\partial r}r\cos\theta\sin\theta\right],\end{aligned} \tag{7}$$

where u is the velocity component in the azimuthal direction, Ω is the rotation rate value, and the notation $\frac{\partial}{\partial z} \equiv \cos\theta \frac{1}{r}\frac{\partial}{\partial \theta} + \sin\theta \frac{\partial}{\partial r}$ denotes the derivative along the direction of the axis of rotation. Note that in the radially symmetric limit, the rhs reduces to only the first term on the rhs, which is exactly the azimuthal component of Eq. (4), giving thermal-wind balance. Equation (7) is an integro-differential equation, since both the gravity, $\mathbf{g_s}$, and $\mathbf{g}'$ are calculated by integrating ρ_s and ρ', respectively. Although this equation can be solved numerically (Galanti et al. 2017), all the additional terms (terms 2-6 on the rhs) are small and contribute very little to the gravity solution. The individual contribution of each of the terms in Eq. (7) is shown in Kaspi et al. (2018) for the case of Jupiter, demonstrating that the first term on the rhs is indeed the leading-order term. All other terms in this equation are at least an order of magnitude smaller, meaning that taking $\mathbf{g} = \mathbf{g}(r)$ and neglecting the centrifugal terms gives the leading-order solution. Galanti et al. (2017) solves the full Eq. (7) and shows that the resulting gravity harmonics are very close to those resulting from using thermal-wind balance.

Consistent with this, Wicht et al. (2020) showed in a theoretical analytical model that beyond J_4 the self-gravity term (term 4 on the rhs of Eq. (7)) indeed contributes less than 10% to the gravity harmonics. For J_3, they found the contribution to be 40%, but they did not take into consideration the compensation due to the other terms in Eq. (7), which are important, particularly since for the lower harmonics the contribution of the centrifugal terms (terms 5 and 6 on the rhs of Eq. (7)) is greater (Cao and Stevenson 2017a). It should be also remembered that other uncertainties—such as assumptions about the exact meridional profile of the zonal wind at depth (see Sect. 4) and its vertical decay profile—have similar contributions. Therefore, dealing with these higher-order contributions associated with planetary oblateness is not necessarily meaningful and will not generally produce a more robust or higher-fidelity gravity result. In any case, solutions that include the self-gravity term (e.g., Zhang et al. 2015; Kong et al. 2018) should retain all the terms on the rhs of Eq. (7) in order to be consistent.

3 The Juno and Cassini Gravity Measurements

The close orbits of Juno and Cassini yielded determination of the gravity harmonics of Jupiter and Saturn to unprecedented accuracy (Iess et al. 2018, 2019). Prior to these missions, the only known gravity harmonics were J_2, J_4 and J_6 (Jacobson 2003; Jacobson et al. 2006). Supplementary Fig. 1 illustrates how much these have been improved over the last few decades, showing the significant reduction in the uncertainty going from the Voyager era to the Juno and Cassini measurements. In addition, the high-order even harmonics J_8 and J_{10} have been now determined with high accuracy (Fig. 2 and Tables 1 and 2). These even harmonics are mostly affected by the interior density distribution and shape of the planet, and only to second order by the flow (ΔJ_n, Eq. (5)), although the relative contribution from the flow increases for the higher harmonics and becomes of similar order to that associated to the rotational flattening beyond J_{10} (Hubbard 1999). Conversely, the odd gravity harmonics (J_3, J_5, J_7, etc.) have no contribution from the interior static density distribution and shape, as these are purely north-south symmetric for such gas planets. The only possible contribution to the odd gravity harmonics comes from hemispheric asymmetries in the dynamics (see the asymmetry in the wind profiles of both Jupiter and Saturn in Fig. 1). Therefore, in terms of probing the dynamics using gravity measurements, the odd harmonics provide a more direct way of determining the depth of the flows (Kaspi 2013).

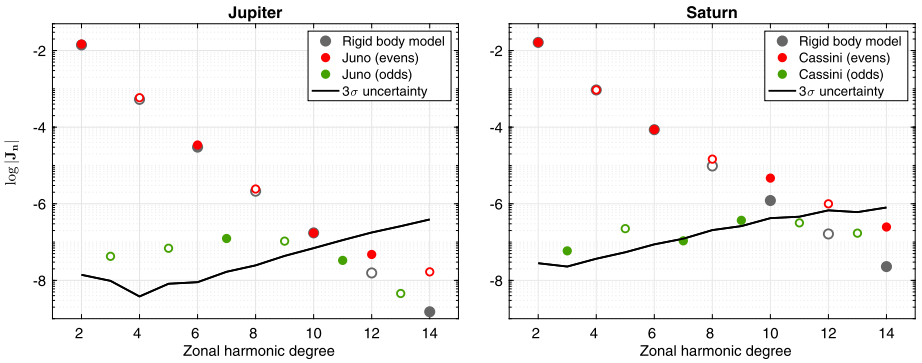

Fig. 2 The measured zonal gravity harmonics of Jupiter and Saturn divided between the even harmonics (red) and odd harmonics (green). For reference, the rigid-body harmonics calculated by the CMS model (Hubbard 1999, 2012) are shown as well (gray). Full circles denote positive values on the log-scale and open circles denote negative values. The lines are the Juno and Cassini 3σ measurement uncertainty (Iess et al. 2018, 2019)

The values of the even harmonics are to leading order powers of q^n, where q is the ratio of the gravity to the centrifugal terms in Eq. (1) (Hubbard 1984). In concert with the internal density distribution, the rotation, therefore, is dominant in determining the gravity harmonic values in the rigid-body limit (no dynamics). The complex dependence on the density distribution can be calculated by interior models (e.g., Hubbard 1975, 1999, 2012; Hubbard and Marley 1989; Nettelmann et al. 2012; Miguel et al. 2016; Hubbard and Militzer 2016), and depends on the equation of state (EOS) as well (e.g., Militzer and Hubbard 2013; Chabrier et al. 2019). Interior models and the EOS are topics of active research and will not be reviewed here, as our focus is on the dynamics (see recent review by Stevenson 2020). Most pre-Juno/Cassini published interior structure models for Jupiter and Saturn gave gravity harmonics that were outside the narrow range of the Juno and Cassini measurements (Supplementary Fig. 1), resulting in a need for improved interior models and EOSs. The first investigation to match the Juno measurements to an internal model was Wahl et al. (2017), who found that the Juno measured harmonics can only be matched if Jupiter has a dilute core that comprises a significant fraction of the planet's radius. These results, however, heavily depend on the choice of the EOS. Recently, Debras and Chabrier (2019) presented a new model for the interior of giant planets and, using a new EOS, were able to match the Juno measurements and the abundance of heavy elements measured by Galileo. Their results also support the existence of an extended dilute core enriched by heavy elements.

Although the dynamical contributions to the even gravity harmonics are small, relative to the rotation and interior mass distribution, they nevertheless exceed the formal measurement uncertainty (supplementary Fig. 1), which is a testament to the high accuracy of the Juno and Cassini gravity measurements. Therefore, in the absence of any knowledge of the mass involved in the flow (i.e., the flow depth), the dynamical effects can be regarded as the effective uncertainty of the gravity harmonics (Kaspi et al. 2017; Debras and Chabrier 2019) for purposes of constraining interior structure models. In Supplementary Fig. 1, we quantify this effective uncertainty, by considering a wide range of possible flow profiles calculated using the method described in Sect. 2 and assuming no a priori knowledge of the internal dynamics (i.e., before the Juno and Cassini measurements). However, given the current knowledge about how deep the cloud-level flows extend, and assuming there are no other significant internal flows that affect the even harmonics, we can obtain more accurate estimates of the

Table 1 Values of Jupiter's $J_2 - J_{10}$ gravity harmonics. Measured values are the Juno measured values, with the uncertainty being three times the formal uncertainty (Iess et al. 2018). The interior model values with no dynamics are averages from the ensemble of rigid-body interior models presented in Guillot et al. (2018). The dynamical contribution is the difference between the measured values and the rigid-body models with no dynamics. The fifth column shows the dynamical solutions when using the cloud-level profile of the zonal wind (Fig. 1), extended down along the direction of the spin axis with a best fit e-folding decay value of $H = 1471$ km (Eq. (8)). The sixth column shows the solutions when using the cloud-level winds, but with a more complex decay function, as described in Kaspi et al. (2018). The seventh column shows the solutions when optimizing both the meridional and vertical profile of the zonal wind (as shown in Fig. 4, blue), with the optimization done for the odd gravity harmonics only (as for columns 5 and 6). The last column shows the same, but with optimization also for the even gravity harmonics (the profiles are shown in Fig. 4, green). The bottom row shows the normalized rms of the difference between the measurements and the solution for all cases, giving a relative value for how close the solution is to the measurements

Jupiter gravity harmonics $\times 10^{-8}$	Juno measurement	No dynamics	Dynamical contribution (ΔJ_n)	Cloud-level flow with simple exponential decay ($H =$ 1471 km)	Cloud-level flow with complex decay function	Adjusted cloud-level flow with complex decay function	Adjusted cloud-level flow with complex decay function. Optimizing both evens and odds
J_2	1469657.22 ± 1.40	1469657.22	0	40.92	54.62	60.11	55.78
J_3	-4.24 ± 0.97	0	−4.24	−7.62	−5.71	−4.25	−4.24
J_4	-58660.92 ± 0.38	−58660.92	0	−5.36	−5.18	−7.34	−4.75
J_5	-6.90 ± 0.82	0	−6.90	−3.19	−7.73	−6.89	−6.90
J_6	3419.80 ± 0.90	3418.80	1.00	1.76	0.33	2.06	1.00
J_7	12.39 ± 1.68	0	12.39	7.47	12.77	12.39	12.39
J_8	-242.58 ± 2.46	−246.08	3.50	2.49	5.41	4.02	3.50
J_9	-10.58 ± 4.35	0	−10.58	−5.38	−8.84	−10.58	−10.58
J_{10}	17.21 ± 6.94	20.21	−3.00	−2.81	−5.36	−4.58	−3.00
rms of fit				3.27	0.94	0.0029	0.00021

effective uncertainty where the dynamical correction to the measurements of the even harmonics is already taken into account. In Supplementary Fig. 1, we show both the effective uncertainty assuming no knowledge of the dynamical contribution (yellow shading) and the dynamical contribution given the knowledge of the flow depth (green dots). For Jupiter, the odd harmonics allow us to obtain an independent measure of the flow depth without any consideration of the even harmonics. For Saturn, in contrast, the even harmonics are needed to determine the flow depth, which makes this effective uncertainty more ambiguous (see Sect. 4).

The even gravity harmonics measured by Juno and Cassini, as well as the theoretical estimates for the gravity values if Jupiter and Saturn were rotating as a rigid body (equivalent to a case where the dynamics are very shallow and have no influence on the gravity field), are presented in Fig. 2 (red and gray dots, respectively). The numerical values for Jupiter and Saturn are presented as well in Tables 1 and 2, respectively. As expected, the low-order even harmonics match previous estimates, as they are mostly dominated by non-dynamical effects, and thus are very close to the rigid body values. For Jupiter, J_8 and J_{10} are also relatively close to the rigid-body values, and therefore the measured even harmonics and

Table 2 Values of Saturn's $J_2 - J_{10}$ gravity harmonics. Measured values are the Cassini Grand Finale measured values, with the uncertainty being three times the formal uncertainty (Iess et al. 2019). The model values without dynamics are the average values from the ensemble of models presented in Galanti et al. (2019). The dynamical contribution is the difference between the measured values and the rigid-body models with no dynamics. The fifth column shows the solutions when using the cloud-level profile of the zonal wind (Fig. 1), extended down along the direction of the spin axis with a best-fit e-folding decay value of $H = 12995$ km (Eq. (8)). The sixth column shows the solutions when using the cloud-level winds, but with a more complex decay function, as described in Galanti et al. (2019). The seventh column shows solutions when optimizing both the meridional and vertical profile of zonal wind (as shown in Fig. 4, green), with the optimization done for the even (J_6, J_8 and J_{10}) and odd gravity harmonics together (as for columns 5 and 6). The last column shows the same, but with the optimization done for the odd harmonics only (the profiles are shown in Fig. 4, blue). The bottom row shows the normalized standard deviation of the difference between the measurements and the solution for all cases, giving a relative value for how close the solution is to the measurements

Saturn gravity harmonics $\times 10^{-8}$	Cassini measurement	No dynamics	Dynamical contribution (ΔJ_n)	Cloud-level flow with simple exponential decay ($H =$ 12955 km)	Cloud-level flow with complex decay function	Adjusted cloud-level flow with complex decay function	Adjusted cloud-level flow with complex decay function. Optimizing with odds only
J_2	1629057.33 ± 2.8	1630000	−142.67	8249.40	8660.38	5053.98	4471.6
J_3	5.89 ± 2.3	0	5.89	−156.92	164.77	8.73	6.20
J_4	-93531.36 ± 3.7	−92576	−955.36	−59.56	49.04	758.83	−386.33
J_5	-22.41 ± 5.4	0	−22.41	72.47	42.83	−25.24	−22.61
J_6	8633.99 ± 8.7	8232.6	401.39	347.23	480.68	409.32	473.01
J_7	10.77 ± 12.2	0	10.77	97.73	127.47	11.04	10.84
J_8	-1462.36 ± 20.5	−922.6	−539.76	−389.30	−558.51	−550.55	−359.29
J_9	36.91 ± 26.0	0	36.91	15.33	45.00	38.06	36.35
J_{10}	467.24 ± 42.0	118.79	348.45	85.69	147.76	366.00	60.63
rms of fit				28.09	28.90	0.610	0.071

the rigid-body values are virtually indistinguishable in Fig. 2. However, for Saturn, these values differ substantially, indicating that the flows extend more deeply than on Jupiter. This separation between the measurements and the rigid-body values matches Hubbard (1999)'s prediction that if a planet is differentially rotating, the even gravity harmonics beyond $n = 8$ will differ from the rigid-body theoretical values. Hubbard's solution allowed only for cases of full differential rotation, meaning the surface flows extend throughout the whole planet (i.e., following the Busse 1976 barotropic model). Intermediate cases for which the surface flows halt at a certain depth can be obtained using methods such as those presented in Sect. 2 (Kaspi et al. 2010). Quantitative solutions, showing which vertical decay profiles best match these measurements, are presented in Sect. 4.

A key result of the Jupiter gravity measurement was that the measured odd gravity harmonics vary significantly from zero—providing the first-ever smoking-gun detection of the effect of flow dynamics on the gravity field of a giant planet. The measured values (green dots in Fig. 2) match predicted theoretical values (Kaspi 2013), calculated by extending the observed cloud-level wind inward along the direction of the spin axis and determining their affect on the gravity field (see Sect. 4). The detection of the zonal flow's expected

gravity signal confirmed that dynamics play a role in redistributing mass inside the planet, and that the dynamics are deep enough to affect the measured gravity field. In contrast with the even gravity harmonics, the odd harmonics receive no contribution from the non-dynamical interior mass distribution, because the equatorial bulge lacks any north-south asymmetries on a gas planet. Conversely, the observed zonal jets do have north-south asymmetries (Fig. 1) and are the only considerable source of north-south asymmetries on the gravity field.

Other sources of north-south asymmetries can be internal oscillations (Durante et al. 2017) and the north-south asymmetry in the magnetic field (Connerney et al. 2018; Moore et al. 2018). However, internal oscillations are expected to give fluctuating contributions from orbit to orbit, whereas the measured odd harmonics are steady. The magnetic effect is expected to scale as the ratio of magnetic pressure to total pressure. For a field of 100 Gauss (plausibly the unobserved toroidal field) in a region of total pressure of ~ 100 kilobars (at ~ 0.96 Jupiter radii), this is of order 3×10^{-9}, likely too small to be important, although it cannot be excluded with complete certainty because this field (unlike the observed poloidal field) is not known. Recently, Kulowski et al. (2020) showed that extreme dynamo velocities beyond 0.1 ms^{-1} are needed to produce a J_3 of the same order of magnitude as that of the measured Juno value, and the contribution to the higher odd harmonics is negligible, implying that the dynamo contribution to the odd harmonics is very small.

For the case of Jupiter, J_3, J_5, J_7 and J_9 were measured to be above the 3-sigma uncertainty level (black line in Fig. 2), while for Saturn only the first two are above the 3-sigma uncertainty level. The robust measurement of Jupiter's odd harmonics, therefore, allows the determination of the depth and structure of the flow, even without consideration of the even harmonics. For Saturn, this issue is less straightforward, because only the first two odd gravity harmonics are above the uncertainty level, and as shown below, those two measurements alone do not give a solution that matches the even harmonics well.

4 Inversion of the Gravity Fields into Wind Fields

Given the measurements from Juno and Cassini, the challenge is to translate these measurements into the wind fields that generate them. The challenge is both in the conversion between the gravity anomaly data and the dynamically balanced wind field and in dealing with the non-unique nature of such solutions. Given that the gravity field is measured by only a finite set of values (Fig. 2), while a full wind field will require many degrees of freedom to be described properly, the solution is obviously not unique (Kaspi et al. 2018). The more degrees of freedom the wind field has, the easier it will be to find a fit to the gravity data. We present therefore a hierarchical approach, beginning with a simple case where the wind is described with only one degree of freedom (and thus a greater number of observables — the gravity harmonics). We then proceed to cases with more degrees of freedom for the wind profile, allowing better matches to the gravity data, but never allowing more degrees of freedom for the wind than the number of overall observables.

We begin with a simple forward model, in which we assume the observed cloud-level flow at the 1-bar level decays radially towards the interior with an e-folding depth defined as H. This represents the expectation that the wind will overall decay with depth (despite possible enhancement in the outermost layers, as measured by the Galileo probe), due to the compressibility of the fluid (Kaspi et al. 2009) and/or Ohmic dissipation at depth due to increasing electrical conductivity (Liu et al. 2008). Due to the dominance of rotation, we extend the cloud-level flow inward along the direction of the spin axis, but the decay itself

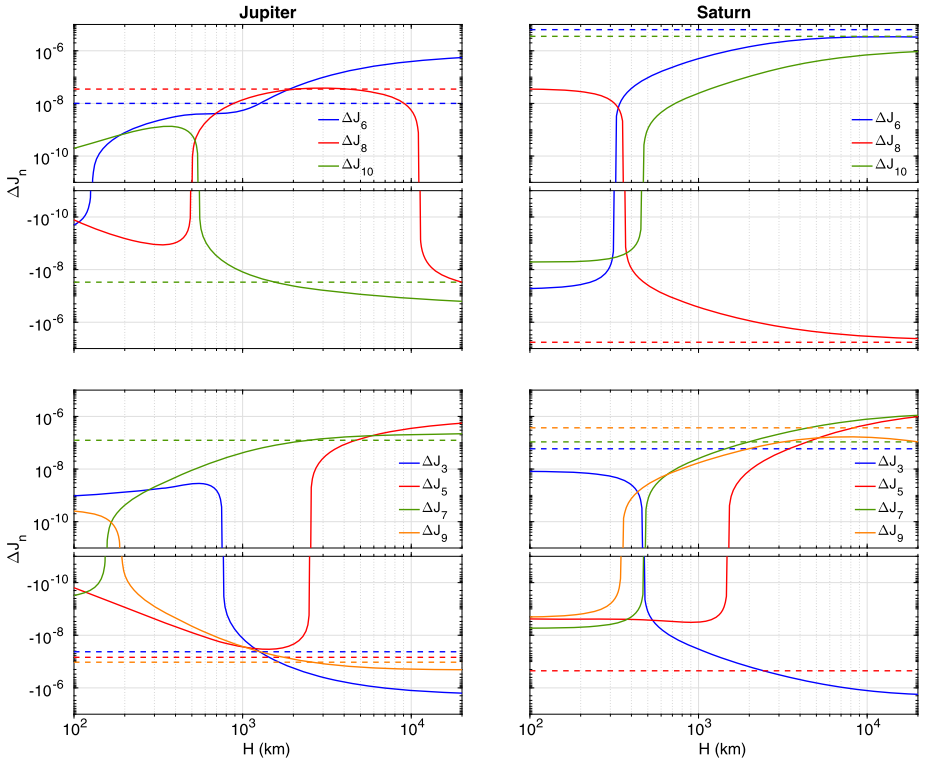

Fig. 3 Theoretical values of the even (top) and odd (bottom) gravity harmonics as a function of the e-folding depth (H) of the cloud-level wind profile for Jupiter (left) and Saturn (right). The solid curves are the predicted dynamical contributions to J_n (Kaspi 2013) for winds decaying exponentially from the measured cloud-top winds given an e-folding depth H. The horizontal, dashed lines are the measured values from Juno and Cassini, where for the even harmonics the rigid-body values used in Tables 1 and 2 have been subtracted. Depth values that match the corresponding measured gravity harmonics correspond to locations where the solid curve crosses the dashed line of the same color

is radial, since the density growth inward is also radial, meaning the functional dependence of the zonal flow is given by

$$u\left(r,\theta\right)=u_{\mathrm{cyl}}\left(r,\theta\right)\exp\left[\left(r-a\right)/H\right], \tag{8}$$

where u_{cyl} is the cloud-level wind profile extended inward along the direction of the axis of rotation, and H is the e-folding radial decay height of this flow (the other parameters are as defined in Sect. 2). Such simplified models for the wind profile have been used in several studies (Kaspi et al. 2010; Kaspi 2013; Liu et al. 2013; Kaspi et al. 2016; Kong et al. 2016a; Guillot et al. 2018).

Given such a zonal wind profile, the zonal component of Eq. (4) is used to generate the gradients of the density anomaly that geostrophically balance this flow profile, and the dynamical gravity harmonics (Eq. (5)) can be obtained. Since the wind profile is asymmetric across the equator, the integration is done separately for the northern and southern hemispheres and then combined, as suggested by Kong et al. (2016b). Figure 3 (solid lines) shows such calculated gravity harmonics as a function of the e-folding depth of the flow, as predicted in Kaspi (2013), for both the even gravity harmonics (top) and the odd harmonics

(bottom). Note that the values of all harmonics switch sign as a function of the depth, depending on how the integrated density structure that is balancing the wind projects onto the different spherical harmonics. Although the sign of these values is not intuitive—the overall tendency to larger values with depth is—due to having more mass involved with the flow. The measured values from Juno and Cassini are shown (dashed lines) on top of the theoretical prediction curves. For the even harmonics, ΔJ_n is calculated as the difference between the measurements and the average rigid-body values from an ensemble of interior models (Guillot et al. 2018; Galanti et al. 2019; see Tables 1 and 2).

For Jupiter, the measured odd harmonics are all negative except for J_7, which is positive, matching the prediction for this simplified model for depths of several thousand kilometers (indicated by the crossing between the solid and dashed lines in Fig. 3). Note that all four gravity harmonics, independently, match the Kaspi (2013) prediction by sign and indicate that the depth of the flow is between 1000 and 3000 kilometers, with the optimized best-fit e-folding depth for all harmonics combined being $H = 1471$ km. Furthermore, the even gravity harmonics (omitting J_2 and J_4 where the relative contribution of the dynamics is very small) show a similar result—all three theoretical curves cross the measurement value between depths of 1500 and 2000 km. The fact that for all seven values (J_3 and J_5–J_{10}), the theoretical calculation matches the Juno measurement in sign and value gives a strong indication that the observed cloud-level flow is related to these measured gravity anomalies and indicates their depth. Nonetheless, using an exponential decay law for the cloud-level winds does not give an exact match to the gravity data (Table 1, column 5), and indeed exponential decay with a uniform e-folding depth was not made based on physical reasoning but for simplicity. Below we present more complex decay functions that better match the measurements, yet the simple model's overall match to the data indicates a strong relationship between the observed flows, their depth and the gravity measurements.

In order to optimize for a more complex decay function, we use an adjoint-based inversion technique (Galanti and Kaspi 2016), where a cost-function is minimized to give a best fit between the decay profile and the gravity measurements, taking into account the uncertainties in the gravity measurements and the error covariance between the different harmonics (Kaspi et al. 2018). Solutions for the vertical decay functions using this method with three degrees of freedom for the shape of the vertical profile (see Kaspi et al. 2018 for details) are shown in Fig. 4. Taking the exact observed cloud-level zonal flows and extending them into the interior with this best-optimized vertical decay function, gives a much better match to the gravity data than the exponential decay function (Table 1, column 6). Next, allowing the optimization procedure to include small variations to the cloud-level wind profile (assuming the zonal wind meridional profile at depth may vary somewhat from what is observed at the cloud level) shows that in this case the solutions give an even better match (Table 1, column 7) to all 4 measured odd gravity harmonics (note that even harmonics are not optimized here, but still give a rather good match). Figure 4 shows that in this case the variations to the observed wind profiles are very minor and well within the uncertainty (and the observed variation between the Voyager and Juno eras) of this profile (Tollefson et al. 2017). The vertical profile in this case (blue) is very similar to the one obtained without varying the meridional structure of the wind profile, indicating again that the strong flows decay at several thousand kilometers depth.

As the odd harmonics are a consequence of the dynamics alone, we have so far used only the odd harmonics for the optimization procedure. Despite this restriction, the resulting even ΔJ_n for these vertical profiles match well both in sign and in magnitude the difference between the measurements of J_6, J_8 and J_{10} and the rigid body values (compare columns 4 and 7 in Table 1). Thus, if we include the even values in the optimization, the results

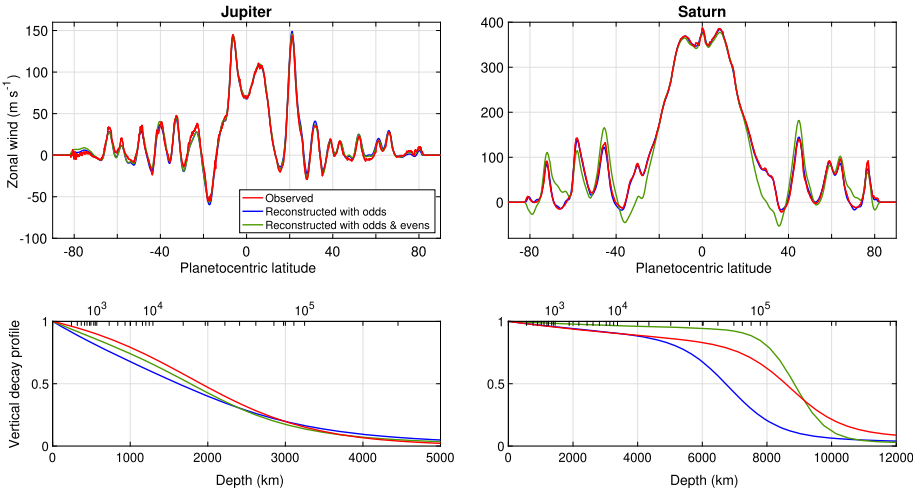

Fig. 4 The optimized meridional profile of the zonal wind (top) for Jupiter (left) and Saturn (right), showing the observed cloud-level wind profile (red), the optimized best fit solutions taking into account the odd harmonics only (blue), and the optimized best fit solutions taking into account both the odd and even harmonics (green). The resulting gravity harmonic values for these profiles appear in Tables 1 and 2. The bottom panel shows the corresponding vertical structures of the zonal flow as a function of the depth (km) and pressure (bar, on the top abscissa)

will not differ substantially. In the final column of Table 1, we present such an optimization, where now all values of the seven gravity harmonics (J_3 and J_5–J_{10}) match exactly the measurements. Here again we allow the wind profile to vary from the observed wind structure, though, as can be seen in Fig. 4, the wind profile needs only minor changes to match the gravity measurements perfectly. We emphasize that this exercise is not unique, and other meridional and vertical profiles of the zonal flow can also potentially give an exact match to the gravity data (Kaspi et al. 2018; Kong et al. 2018). However, following Occam's razor reasoning, we have shown here that taking the *observed* cloud-level flow and extending it inward in a very simple fashion gives an exact match to the gravity measurements. Duer et al. (2020) explore a wide range of possible interior zonal flow profiles, varying both in latitude and vertically, and show that while it is possible to find solutions with a zonal wind profile different from that at the cloud level, solutions that differ from the cloud-level flow substantially are statistically unlikely.

Complementary to this analysis, Guillot et al. (2018) used a wide range of rigid-body models for Jupiter (without averaging, as in Table 1, column 3) to calculate the possible range of dynamical contributions to the even zonal harmonics, by subtracting this range of rigid-body solutions from the Juno gravity measurements. This range was used to constrain a wide range of hypothetical flow profiles, with different e-folding decay depths and not bounded to the observed cloud-level flows, derived using thermal wind balance (as in Kaspi et al. 2017). This analysis, consistent with the analysis presented above, showed that with high likelihood the flow extends down to $2000-3500$ km beneath the cloud level, regardless of its specific meridional structure. Although the Guillot et al. (2018) analysis is not sensitive to the detailed vertical-decay profile of the flow, nor can it constrain the meridional profile of the zonal flow, it gives an independent method for constraining the bulk depth of the flow using the even gravity harmonics alone. Given the match of the flow to the even gravity

harmonics, it also indicates that the flow beneath this layer is likely weak (< 5 m s^{-1}); otherwise, it would influence the measured even gravity harmonics.

For Saturn, the cloud-level flow has shown possible variability between the Voyager and the Cassini eras, and overall the zonal flow velocities are less certain (García-Melendo et al. 2011), particularly at low latitudes, where the powerful equatorial jet lies. Repeating the same analysis as for Jupiter and taking the cloud-level flow of García-Melendo et al. (2011) with a simple exponential decay gives a relatively good match to the even harmonics (same sign and within a factor of 2 in magnitude) for e-folding depths of $\sim 10^4$ km. This indicates a substantially deeper flow than for Jupiter. The odd harmonics for Saturn, despite being similar in magnitude to those of Jupiter, are closer to the measurement uncertainty and, therefore, only J_3 and J_5 have significant values (Fig. 2). Both, however, have an opposite sign compared to the theoretical prediction when using the cloud-level wind profile (Fig. 3), indicating that a more sophisticated model is needed for Saturn. Similarly, using the cloud-level winds and allowing for a more complex decay profile does not give a good match to the gravity measurements (Table 2, column 6). This suggests that the latitudinal dependence of the zonal winds at depth differs from that measured by cloud-tracking in the atmosphere. Consistent with this idea, when the meridional profile of the zonal wind at depth is allowed to deviate from the observed (cloud-tracked) profile, a good match to the measurements can be found (Fig. 4, green profile). Note that, similar to the Jupiter case, here we do not try to fit for J_2 and J_4, since the dynamical contribution is small relative to the rigid body (Galanti et al. 2019).

The deviation from the observed cloud-tracked wind profile of Saturn is mainly around latitude 30°, where the flow needs to be more westward than the observed cloud-level wind, with values ~ 50 m s^{-1}, in order to match the measurements for both the even and odd harmonics (Table 2, column 7). The match is obtained with a vertical profile that is nearly barotropic down to ~ 8000 km and then decays with depth (green profile in Fig. 4) (Galanti et al. 2019). A similar conclusion, that a westward flow around latitude 30° is needed in order to match the even gravity harmonics, was also reached by Militzer et al. (2019), who used a model that allows the flow to extend inward only barotropically (without changing along the direction of the spin axis), and found that such a westward zonal flow profile is needed to match the measurements. Based on theoretical arguments alone, Chachan and Stevenson (2019) obtained a similar conclusion, that a retrograde wind profile is necessary around latitude 30° in order to match the measurements. The optimizations discussed here used both the values of the odd and the even harmonics and took into account all cross-correlations. For Saturn, optimizing only with odd harmonics does not give a good match to the even harmonics, highlighting the difference between Jupiter and Saturn and demonstrating that for Saturn, the high-order even harmonics (particularly J_8 and J_{10}) are key to determining the depth and profile of the deep flows. The uncertainty in rotation rate affects only the dynamical J_2 and J_4 and thus is not important for interpreting the Saturn gravity measurements (Galanti and Kaspi 2017).

Comparing the different columns in Tables 1 and 2 and considering the different profiles in Fig. 4 shows that the gravity results not only inform us about the depth of the jets, but also about the meridional profile of the zonal flow at depth. The results show that the measurements are sensitive to the exact meridional profile, although the variations to it that are needed to get exact matches are not significant. To test the statistical significance of this profile (on Jupiter), other profiles with a different meridional profile of the zonal flow have been assessed to investigate the possibility that the flow at depth might exhibit major qualitative differences from the flow observed at cloud level. Out of a sample of a thousand zonal-wind profiles as a function of latitude with the same overall amplitude but different meridional

profiles, less than 1% have a better match to the measurements using the same optimization procedure (Kaspi et al. 2018). These few profiles had no correlation to one another, nor to the cloud-level profile. This indicates that although such random solutions can be found, it is with high confidence that the meridional profile of the zonal flow observed at the cloud level extends to depth (see also Duer et al. 2020).

5 Interaction of the Flow with the Magnetic Field at Depth

The results presented above have shown some key similarities and differences between Jupiter and Saturn. On both planets, the measured gravity harmonics indicate how deep the cloud-level flows extend, and give a good match to a zonal wind profile at depth that is very similar to the one observed at the cloud level. While on Jupiter the jets extend down to ~ 3000 km, on Saturn that depth nearly triples (Fig. 5). However, note that the mass of Jupiter is 3.3 times that of Saturn, while the radius is only about 1.2 times larger, resulting in mean density and surface gravitational acceleration on Jupiter that are 2–3 times larger than those of Saturn. As a consequence, the electrical conductivity of Saturn only achieves large values at a much greater depth than it does on Jupiter (Fig. 5 red dashed lines in the top panels). Thus, despite the different depths, in both cases the rise in electrical conductivity occurs near 10^5 bar, due to the dependence of electrical conductivity on temperature (Stevenson 2003). Strikingly, the depth where the electrical conductivity rises in both planets is at the same depth where the gravity measurements imply that the zonal winds decay (where the blue and red curves cross in Fig. 5). This strongly hints that Ohmic dissipation plays a role in damping the flow at depth, and in fact was predicted previously based on theoretical arguments (Liu et al. 2008; Cao and Stevenson 2017b).

As a consequence of Saturn being less dense than Jupiter, the depth at which a particular pressure is reached in Saturn is about three times greater than the corresponding depth for Jupiter. The temperature at a given pressure is only modestly ($\sim 20\%$) lower in Saturn than in Jupiter. Temperature is most important for determining the electrical conductivity of hydrogen, which results from the excitation of electrons across the band gap between valence and conduction states (Stevenson and Salpeter 1977). This conductivity is an extremely strong function of temperature, both in theoretical (French et al. 2012) and experimental results (Nellis et al. 1992), which are essentially in agreement. The expected conductivity at 3000 km in Jupiter and 9000 km in Saturn (about 10^5 bars in both planets) is approximately 1 $\mathrm{S\,m^{-1}}$ (similar to that of salty water at room temperature). At this level of conductivity, strong zonal winds would create a toroidal magnetic field whose associated electrical currents would produce a total Ohmic dissipation that is comparable to the observed luminosity of the planets (Liu 2006; Liu et al. 2008).

The factor-of-three difference in zonal wind depth between Jupiter and Saturn, together with a remarkable correspondence to the theoretical argument of Liu et al. (2008) (their prediction was 2800 km for Jupiter), strongly suggests the role of magnetohydrodynamics in controlling the depth of the zonal jets. It should also be noted that because the electrical conductivity is such an extremely strong function of temperature and, therefore, radius, the results hold even given a likely order-of-magnitude uncertainty in the electrical conductivity, as well as the large difference in magnetic field strength between Jupiter and Saturn. Nonetheless, the Lorentz force is not sufficient by itself to dampen the flows from large values (tens of $\mathrm{m\,s^{-1}}$) to zero (Cao and Stevenson 2017b).

Therefore, although the Ohmic dissipation might be the ultimate process that halts the flow at depth, it does not explain the gradual diminishment in zonal-flow speed from the

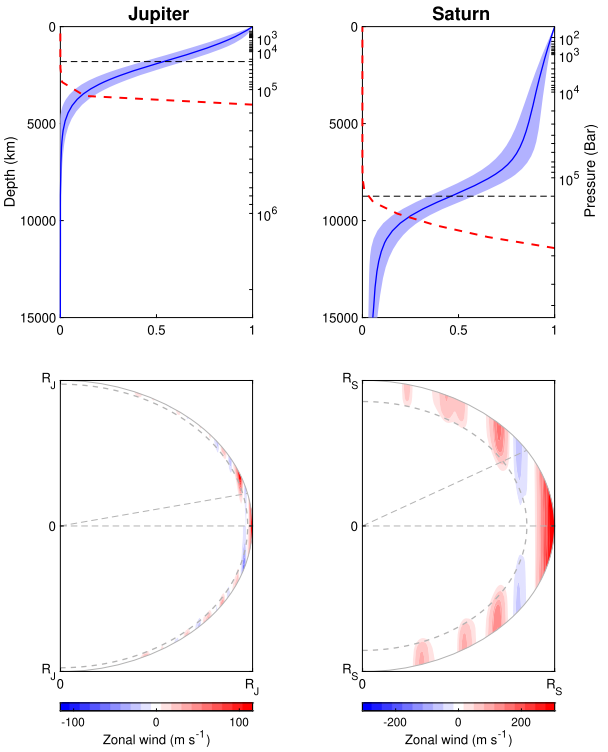

Fig. 5 The vertical structure of the zonal flow on Jupiter (left) and Saturn (right) as function of depth, corresponding to the best fit profile presented in column 6 of Table 1 and column 7 of Table 2, respectively. The upper panel shows this vertical decay profile (blue), its uncertainty (blue shading) and the electrical conductivity profile (red dashed) as given by Liu et al. (2008) for Jupiter and French et al. (2012) for Saturn. The electrical conductivity is in units of S m^{-1}, with the scale going linearly from 0 to 100. The middle point in the decay profile, at depths of 1831 km and 8743 km for Jupiter and Saturn, respectively, is marked by the dashed horizontal line. The bottom panel show the zonal flow profile (m s^{-1}) as a function of latitude and depth in the spherical projection. The middle point corresponding to that shown in the upper panels appears as the thick dashed line. The thin dashed lines contain the angle (latitude) derived from extending the depth of the flow along the direction of the spin axis ($\theta_e = \cos^{-1}(x/a)$, where a is the planetary radius and x is the depth beyond the middle point of the flow profile). This latitude (θ_e) is 13° for Jupiter and 31° for Saturn, close to the latitude where the flow is observed to turn from eastward to westward at the cloud level

cloud level down to depths where the electrical conductivity becomes large (Fig. 5). In this region, the dissipation of the zonal flow and its gradual decay with depth must result from other mechanisms (Christensen et al. 2020). Elucidating these mechanisms requires an understanding of how convective heating is organized throughout the envelope, setting the entropy distribution that is in thermal wind balance with the zonal flows (Eq. (9)). A key for understanding this issue is the eddy-driven meridional circulation, which might be playing an important in organizing the heat distribution (see below). In analogy to Earth's atmospheric dynamics, eddy fluxes in the upper atmosphere force a meridional circulation that redistributes heat, and the jet structure adjusts to be in balance with the heat distribution (Schneider and Liu 2009).

Reorganization of Eq. (4), looking at its zonal component and assuming the background profile is adiabatic leads to a relation between the wind shear along the direction of the spin

axis and the entropy gradients (Kaspi et al. 2009):

$$\frac{\partial u}{\partial z} = -\frac{g}{2\Omega\rho_s}\left(\frac{\partial \rho}{\partial s}\right)_p \frac{1}{r}\frac{\partial s'}{\partial \theta}, \tag{9}$$

where s is the specific entropy. Thus the direction of the shear is determined by the average sign of the entropy anomaly gradients, and the shear is expected to be largest at the lower depths, where the entropy expansion coefficient, $\frac{1}{\rho_s}\left(\frac{\partial \rho}{\partial s}\right)_p$, is smallest, mostly because the large increase in density with depth. Liu et al. (2013) suggested that if convection is aligned mainly with the direction of the spin axis, as seen in numerical simulations of deep convective atmospheres (Kaspi 2008; Aurnou et al. 2008), the entropy gradients in Eq. (9) will then be dominated by those perpendicular to the direction of the spin axis, since $\frac{1}{r}\frac{\partial s}{\partial \theta} = \cos\theta\frac{\partial s}{\partial z} + \sin\theta\frac{\partial s}{\partial r_\perp}$, and $\frac{\partial s}{\partial r_\perp} \gg \frac{\partial s}{\partial z}$, where $r_\perp$ is the direction perpendicular to the spin axis. Following Liu et al. (2013), if the entropy gradients in the direction of the spin axis are identically zero ($\frac{\partial s}{\partial z} = 0$) along cylinders parallel to the spin axis, throughout the depth of the zonal flows, then $\frac{\partial s}{\partial r_\perp}$ is constant along the same cylinders, implying $\frac{\partial u}{\partial z}$ in Eq. (9) can be determined given the entropy expansion coefficient. This suggests a physical argument for the functional decay in the wind profile with depth, but the implied wind profile does not match the gravity harmonic values for both Jupiter and Saturn (Liu et al. 2013, 2014), likely because the assumption that $\frac{\partial s}{\partial z} = 0$ throughout the depth of the flow is very strict and not satisfied in the interiors of Jupiter and Saturn. Nonetheless, a physical argument for the dependence of $\frac{\partial s}{\partial \theta}$ on depth and latitude is key for a theory for the vertical profile of the zonal wind.

In the purely barotropic limit, the rhs of Eq. (9) vanishes, and the flow is then purely aligned with the axis of rotation. This is similar to the Taylor-Proudman theorem (Pedlosky 1987), although the formal theorem requires the fluid to be incompressible, in which case all three components of velocity are aligned with the rotation axis ($2\Omega \cdot \nabla \mathbf{u} = 0$). For a compressible flow, in the barotropic limit, the alignment is for the zonal and meridional component of the flow (throughout this paper, only the zonal component of the velocity is discussed). Yet, due to the entropy gradients (Eq. (9)), and as evident from the gravity results, the flow is likely not fully barotropic (baroclinic). Qualitatively, however, the velocity on both planets varies by O(100 m s^{-1}) over thousands of kilometers, implying that the flows in effect are not very far from barotropic. If we assume the variation from barotropy is large, and allow the observed flows to extend inward in a different way (e.g., radially), the match to the gravity measurements would not have been as good as shown in Tables 1 and 2. For example, extending the cloud-level flow inward radially for Jupiter results in J_3 changing sign. In this case, solutions matching the data can be found only if the meridional variation of zonal flow at depth differs substantially from that at the cloud level.

The deep thermal structure set by Eq. (9) needs to be considered in combination with the forcing mechanism of the zonal flow. Terrestrial atmospheric dynamics gives a clear understanding that geostrophic turbulence on a rotating planet will drive turbulent eddy momentum fluxes, resulting in regions of momentum flux convergence with eastward (prograde) flows and momentum flux divergence with westward (retrograde) flows. Cloud-tracking analyses for both Jupiter (Salyk et al. 2006) and Saturn (Del Genio et al. 2007) show that, indeed, regions of eddy momentum flux convergence (divergence) are strongly correlated with the eastward (westward) jets, implying this is a plausible mechanism for driving the zonal flows. Yet, the sources of the eddies are not known, although potential candidates have been identified as barotropic or baroclinic instabilities (e.g., Kaspi and Flierl 2007; Lian and Showman 2008; Schneider and Liu 2009; Liu and Schneider 2010; Young et al.

2019) or the internal convection itself (e.g., Heimpel et al. 2005; Young et al. 2019; Showman et al. 2019). It has also been shown that both shallow and deep forcing can drive such zonal flows (Showman et al. 2006).

The driving and dissipation mechanisms discussed here can be considered in a single expression by taking the leading component of the momentum equation (Eq. (1)) and expressing it in terms of angular momentum (Vallis 2017). Taking a zonal and vertical average in steady state gives,

$$\mathbf{u} \cdot \nabla M = -S + D, \tag{10}$$

where $M = \Omega r^2 \cos^2\theta + ur\cos\theta$ is the total angular momentum, $S = \mathbf{u}' \cdot \nabla M'$ is the eddy angular momentum flux divergence and D is the Lorentz drag (Schneider and Liu 2009). In regions of low electrical conductivity, closer to the cloud level, the balance will be $\mathbf{u} \cdot \nabla M = -S$, meaning the eddy momentum flux convergence drives the meridional flow across angular momentum surfaces (i.e., across the direction of the spin axis) to force the meridional circulation. In this momentum balance, momentum flux convergence (eastward jet) is balanced by an equatorward flow, and momentum flux divergence (westward jet) is balanced by a poleward flow. In the deep region, where the electrical conductivity increases sufficiently (Fig. 5), the drag allows for cross-angular momentum flow, $\mathbf{u} \cdot \nabla M = D$, to close the circulation. Thus, the meridional flow will be opposite to the flow aloft. In between, Eq. (10) reduces to $\mathbf{u} \cdot \nabla M = 0$, meaning there is no flow across angular momentum surfaces, so the flow must be along cylinders aligned with the direction of the axis of rotation. This constraint, that $\mathbf{u} \cdot \nabla M = 0$, does not put a direct constraint on how barotropic the zonal flow is, but indirectly puts a strong constraint on the meridional circulation, which affects the entropy gradients in Eq. (9), and through this the zonal wind shear. This expression of the meridional circulation is similar to those used to explain the midlatitude Ferrel cell on Earth, with surface drag taking the place of the Lorentz drag (Vallis 2017).

The dynamical constraints discussed earlier suggest that the flow extends inward along the direction of the spin axis, as demonstrated in Fig. 5, where the full solution for the zonal wind in the radial-latitudinal plane is presented. Evidently, for the case of Jupiter, despite the jets being deep from an atmospheric perspective, extending down to $\sim 10^5$ bar and advecting 1% of the mass of the whole planet (Fig. 6), from the point of view of the whole gaseous planet, and compared to the proposed Busse (1976) model scenario, the winds penetrate through only a small fraction of the planet. For Saturn, the fraction is larger, going down to 15% of the radius of the planet, but still containing only a few percent of the total mass (Fig. 6). That said, on both planets, the atmospheric advection of several percent of the planetary mass is very significant, and by far exceeds the advection on any other planet in the solar system (e.g., Earth's atmosphere is less than one part in a million of the overall planetary mass).

Interestingly, the depths of the winds of both Jupiter and Saturn, obtained from the gravity measurements, are also consistent with the observed latitudinal extent of the equatorial eastward flow, meaning that if the depth of the flow at the equator is extended along the direction of the axis of rotation, it intersects the surface almost exactly at the latitude where the zonal flow first turns from positive to negative (eastward to westward). Quantitatively, taking the half point of the flow profile structure at the equatorial plane (horizontal lines in the top panels of Fig. 5), which are 1831 km deep for Jupiter and 8743 km deep for Saturn, and calculating the latitude where this line intersects the surface gives a latitude of 13° for Jupiter and 31° for Saturn. This is very close to the latitude where the equatorial flow changes sign, which is 13° and 35° for Jupiter and Saturn, respectively. Note that for

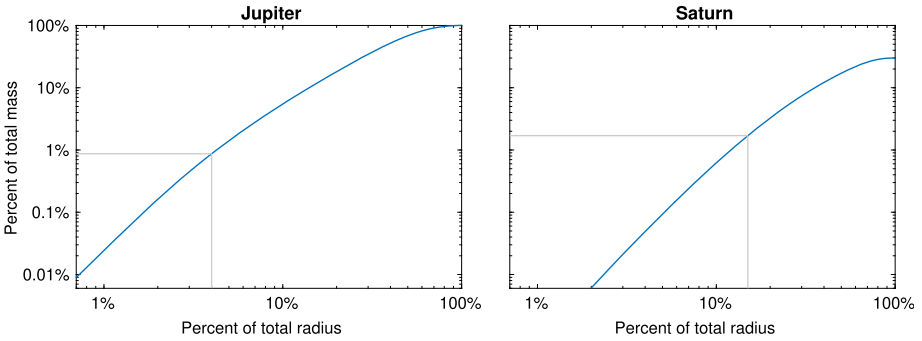

Fig. 6 The percentage of Jupiter's (left) and Saturn's (right) mass as a function of depth beneath the 1-bar level. The grey line shows the percentage of mass contained within the depth of the zonal flows as found by the gravity measurements

Saturn, if a rotation rate of 10:34 is taken instead of 10:39, as recent publications indicate, this latitude changes to 31° (Fig. 1). Thus, the coincidence between the tangent cylinder's intersection with the surface and the end of the equatorial prograde jet gives another independent observation that is in agreement with the conclusion from the gravity measurements regarding the depth of the zonal jets. Such arguments regarding the depth of the equatorial superrotation region have been presented in the past in the context of the tangent cylinder surrounding the inner region of deep convective models (e.g., Heimpel et al. 2005; Aurnou et al. 2008; Kaspi et al. 2009; Liu and Schneider 2010; Gastine et al. 2013).

6 The Depth of the Zonal Flow on Uranus and Neptune

As on Jupiter and Saturn, Uranus and Neptune also have very strong east-west flows at the observed cloud level. These flows reach $\sim 200\ \mathrm{m\,s^{-1}}$ on Uranus and nearly $400\ \mathrm{m\,s^{-1}}$ on Neptune, with a meridional structure that is overall similar between the two planets, consisting of a westward broad equatorial flow and a strong and broad eastward flow at midlatitudes. The flows have an overall similar character despite the planetary obliquity being very different (98° on Uranus and 29° on Neptune), and the internal heat flux being three times stronger than the solar flux on Neptune, while on Uranus the internal heat flux appears to be negligible (Pearl et al. 1990; Pearl and Conrath 1991). As these are the only two planets yet to host a dedicated space mission (Fletcher et al. 2020b), most data comes from the Voyager 2 encounters of the two planets in 1986 and 1989 (Smith et al. 1986, 1989). The data obtained from Voyager includes the gravity harmonics up to J_4, although to a much lesser precision than the Juno and Cassini data discussed above (Jacobson 2007, 2009). Nonetheless, due to the broader latitudinal structure of the zonal wind, and its relative resemblance to the latitudinal structure of P_4 (Eq. (5)), an upper bound can be placed on the depth of the atmospheric circulation on these two planets (Kaspi et al. 2013).

The upper limit on the depth of circulation was placed by utilizing the known values of J_4 from Voyager and determining the difference between the observed J_4, and the J_4 resulting from a wide range of rigid-body models set to match all other observational constraints besides J_4. Any difference in these quantities places constraints on the dynamical contribution to J_4. Therefore, considering the observed J_4 and its uncertainty and the widest possible range of J_4 solutions from interior models, ranging from models with no solid cores to ones

with massive solid cores (Helled et al. 2010, 2011; Nettelmann et al. 2013), an upper limit to the dynamic contribution to J_4 (ΔJ_4, as in Eq. (5)) was constructed. This revealed that the dynamics are constrained to the outermost 0.4% of the mass on Uranus and 0.2% on Neptune, providing a much stronger limitation to the depth of the dynamical atmosphere than previously suggested (Hubbard et al. 1991). This result implies that the dynamics must be confined to a thin weather layer of no more than 1600 km on Uranus and 1000 km on Neptune (Kaspi et al. 2013). This is much shallower than the depths on Jupiter and Saturn, with the pressure to which the flows extend being at most 4000 bar on Uranus and 2000 bar on Neptune.

7 Discussion and Conclusion

The recent gravity measurements of Juno and Cassini have provided data accurate enough to allow key inferences on the effect of atmospheric dynamics on the gravity field of both planets. Analysis of these measurements has yielded estimates of the depth of the strong zonal flows on both planets, and implies that the meridional profile of the zonal flows observed at the cloud level of both planets likely extends to great depths. An intrinsic problem of any gravity inversion is that the contributing field is not unique, meaning in this case that the wind-induced gravity anomalies cannot be traced uniquely to the wind field creating them. However, there are several independent lines of evidence supporting the solutions presented here:

1. The simplest possible Jovian flow model, taking the observed cloud-level winds and extending them inward, matches all 4 measured odd gravity harmonics (J_3, J_5, J_7 and J_9) independently both in sign and in magnitude (Fig. 3).
2. The same wind profile matches the dynamical component of the even gravity harmonics (J_6, J_8 and J_{10}) as well (Fig. 3).
3. Other than atmospheric dynamics, no other source is likely to produce north-south asymmetries that give rise to the observed magnitudes of the odd gravity harmonics (Sect. 5).
4. Repeating the analysis presented here, using random zonal wind profiles (considering that the cloud-level winds may be decoupled from the interior flow causing the measured gravity anomalies), shows that less than 1% of such wind profiles give a match to the gravity measurements (Kaspi et al. 2018). In other words, the vast majority of possible zonal-wind profiles for the winds at depth yield a much worse fit to the gravity data than simply extending the observed zonal-wind profile inward (Duer et al. 2020).
5. The Saturnian winds, with slight modifications (within the error range of the wind measurements), match the dynamical component of the gravity measurements for both the even (J_6, J_8 and J_{10}) and odd harmonics (Fig. 4).
6. For both Jupiter and Saturn, the depth of the flows inferred from the gravity measurements matches the depth where electrical conductivity rises abruptly (Fig. 5). This suggests that the previously suggested mechanism of Ohmic dissipation might play a key role in setting the flow depth (Liu et al. 2008).
7. For both Jupiter and Saturn, the depth of the flows inferred from the gravity measurements matches the depth inferred from a tangent cylinder separating the equatorial eastward flow and the higher latitude flows. This may explain the different latitudinal extent of the equatorial flow on both planets (Fig. 5).
8. Temporal variation of the magnetic field of Jupiter implies that the variation is carried by the zonal flow and gives a magnitude of the zonal flow at depth that is very small,

and consistent with the overall depth implied by the gravity measurements (Moore et al. 2019).

Although each of these lines of evidence could individually perhaps be challenged as being coincidental, when taken together, they yield a coherent picture regarding the extent and character of the flows beneath the cloud level of Jupiter and Saturn. On both planets, the flows advect a substantial part of the mass of the planets ($1-2\%$), greater than in any other planetary atmosphere (Fig. 6). This depth implies that the flows span from top to bottom, nearly four orders of magnitude in density and nearly six orders of magnitude in pressure. That said, the depth on both planets is just a small fraction of the planetary radius ($\sim 4\%$ on Jupiter and $\sim 15\%$ on Saturn), suggesting that from a planetary perspective the flows are still bound to a relatively shallow layer.

Despite this new understanding regarding the depth and structure of the flow, we are still left with an incomplete picture of the mechanisms driving the flow. Particularly, several open questions remain, such as, What causes the flow to decay before reaching the Ohmic dissipation level at $\sim 10^5$ bar? What drives the equatorial superrotation? Why are the flows on Saturn substantially stronger? What is the source of the eddies driving the jets? What are the roles of baroclinic, barotropic and convective instabilities in driving the winds? With better constrains on the dynamical component of the gravity fields (due to improved interior models), magnetic fields and their secular variation (with more Juno orbits, Duer et al. 2019), and temperature fields and water abundance (Juno microwave measurements, Li et al. 2020) as well as improved dynamical models, these questions might be addressed in the coming years, to give a better understanding of the fundamental physical processes driving the dynamics on the giant planets.

Acknowledgements Kaspi and Galanti acknowledge support by the Israeli Space Agency and the Helen Kimmel Center for Planetary Science at the Weizmann Institute of Science. All authors acknowledge support by the Juno project. We are extremely grateful to Kunio Sayanagi and an anonymous reviewer for their helpful comments. We acknowledge support from the Understanding the Diversity of Planetary Atmospheres workshop at the International Space Science Institute (ISSI) in November 2018 for inspiring this review.

References

J.D. Anderson, G. Schubert, Saturn's gravitational field, internal rotation, and interior structure. Science **317**, 1384–1387 (2007)

D.H. Atkinson, J.B. Pollack, A. Seiff, Galileo Doppler measurements of the deep zonal winds at Jupiter. Science **272**, 842–843 (1996)

J.M. Aurnou, P.L. Olson, Strong zonal winds from thermal convectionin a rotating spherical shell. Geophys. Res. Lett. **28**(13), 2557–2559 (2001)

J. Aurnou, M. Heimpel, L. Allen, E. King, J. Wicht, Convective heat transfer and the pattern of thermal emission on the gas giants. Geophys. J. Int. **173**, 793–801 (2008)

S.J. Bolton, Juno Final Concept Study Report. Technical Report AO-03-OSS-03 New Frontiers, NASA (2005)

S.J. Bolton, A. Adriani, V. Adumitroaie, M. Allison, J. Anderson, S. Atreya, J. Bloxham, S. Brown, J.E.P. Connerney, E. DeJong, W. Folkner, D. Gautier, D. Grassi, S. Gulkis, T. Guillot, C. Hansen, W.B. Hubbard, L. Iess, A. Ingersoll, M. Janssen, J. Jorgensen, Y. Kaspi, S.M. Levin, C. Li, J. Lunine, Y. Miguel, A. Mura, G. Orton, T. Owen, M. Ravine, E. Smith, P. Steffes, E. Stone, D. Stevenson, R. Thorne, J. Waite, D. Durante, R.W. Ebert, T.K. Greathouse, V. Hue, M. Parisi, J.R. Szalay, R. Wilson, Jupiter's interior and deep atmosphere: the initial pole-to-pole passes with the Juno spacecraft. Science **356**, 821–825 (2017)

F.H. Busse, Thermal instabilities in rapidly rotating systems. J. Fluid Mech. **44**, 441–460 (1970)
F.H. Busse, A simple model of convection in the Jovian atmosphere. Icarus **29**, 255–260 (1976)
F.H. Busse, Convection driven zonal flows and vortices in the major planets. Chaos **4**(2), 123–134 (1994)
J.K. Campbell, J.D. Anderson, Gravity field of the Saturnian system from Pioneer and Voyager tracking data. Astrophys. J. **97**, 1485 (1989)
J.K. Campbell, S.P. Synnott, Gravity field of the Jovian system from pioneer and Voyager tracking data. Astrophys. J. **90**, 364–372 (1985)
H. Cao, D.J. Stevenson, Gravity and zonal flows of giant planets: from the Euler equation to the thermal wind equation. J. Geophys. Res., Planets **122**, 686–700 (2017a)
H. Cao, D.J. Stevenson, Zonal flow magnetic field interaction in the semi-conducting region of giant planets. Icarus **296**, 59–72 (2017b)
G. Chabrier, S. Mazevet, F. Soubiran, A new equation of state for dense hydrogen-helium mixtures. Astrophys. J. **872**, 51 (2019)
Y. Chachan, D.J. Stevenson, A linear approximation for the effect of cylindrical differential rotation on gravitational moments: application to the non-unique interpretation of Saturn's gravity. Icarus **323**, 87–98 (2019)
R. Chemke, Y. Kaspi, The latitudinal dependence of atmospheric jet scales and macroturbulent energy cascades. J. Atmos. Sci. **72**, 3891–3907 (2015)
J. Cho, L.M. Polvani, The formation of jets and vortices from freely-evolving shallow water turbulence on the surface of a sphere. Phys. Fluids **8**, 1531–1552 (1996)
D.S. Choi, A.P. Showman, R.H. Brown, Cloud features and zonal wind measurements of Saturn's atmosphere as observed by Cassini/VIMS. J. Geophys. Res., Planets **114**(E4), 04007 (2009)
U.R. Christensen, Zonal flow driven by deep convection in the major planets. Geophys. Res. Lett. **28**, 2553–2556 (2001)
U.R. Christensen, J. Wicht, W. Dietrich, Mechanisms for limiting the depth of zonal winds in the gas giant planets. Astrophys. J. **890**(1), 61 (2020)
J.E.P. Connerney, S. Kotsiaros, R.J. Oliversen, J.R. Espley, J.L. Joergensen, P.S. Joergensen, J.M.G. Merayo, M. Herceg, J. Bloxham, K.M. Moore, A new model of Jupiter's magnetic field from Juno's first nine orbits. Geophys. Res. Lett. **45**(6), 2590–2596 (2018)
F. Debras, G. Chabrier, New models of Jupiter in the context of Juno and Galileo. Astrophys. J. **872**, 100 (2019)
A.D. Del Genio, J.M. Barbara, J. Ferrier, A.P. Ingersoll, R.A. West, A.R. Vasavada, J. Spitale, C.C. Porco, Saturn eddy momentum fluxes and convection: first estimates from Cassini images. Icarus **189**(2), 479–492 (2007)
K. Duer, E. Galanti, Y. Kaspi, Analysis of Jupiter's deep jets combining Juno gravity and time-varying magnetic field measurements. Astrophys. J. Lett. **879**(2), 22 (2019)
K. Duer, E. Galanti, Y. Kaspi, The range of Jupiter's flow structures fitting the Juno asymmetric gravity measurements. J. Geophys. Res., Planets (2020, in press). https://doi.org/10.1029/2019JE006292
D. Durante, T. Guillot, L. Iess, The effect of Jupiter oscillations on Juno gravity measurements. Icarus **282**, 174–182 (2017)
D. Durante, M. Parisi, D. Serra, M. Zannoni, V. Notaro, P. Racioppa, D.R. Buccino, G. Lari, L. Gomez Casajus, L. Iess, W.M. Folkner, G. Tommei, P. Tortora, S.J. Bolton, Jupiter's gravity field halfway through the Juno mission. Geophys. Res. Lett. **47**(4), e2019GL086572 (2020)
S.G. Edgington, L.J. Spilker, Cassini's grand finale. Nat. Geosci. **9**, 472–473 (2016)
L.N. Fletcher, P.G.J. Irwin, N.A. Teanby, G.S. Orton, P.D. Parrish, R. de Kok, C. Howett, S.B. Calcutt, N. Bowles, F.W. Taylor, Characterising Saturn's vertical temperature structure from Cassini/CIRS. Icarus **189**(2), 457–478 (2007)
L.N. Fletcher, Y. Kaspi, T. Guillot, A.P. Showman, How well do we understand the belt/zone circulation of giant planet atmospheres? Space Sci. Rev. **216**(2), 30 (2020a)
L.N. Fletcher, N. André, D. Andrews, M. Bannister, E. Bunce, T. Cavalié, S. Charnoz, F. Ferri, J. Fortney, D. Grassi, L. Griton, P. Hartogh, R. Helled, R. Hueso, G. Jones, Y. Kaspi, L. Lamy, A. Masters, H. Melin, J. Moses, O. Mousis, N. Nettleman, C. Plainaki, E. Roussos, J. Schmidt, A. Simon, G. Tobie, P. Tortora, F. Tosi, D. Turrini, Ice giant systems: the scientific potential of missions to Uranus and Neptune. Planet. Space Sci. (2020b, in press)
W. Folkner, L. Iess, P. Tortora more, Jupiter gravity field from first two orbits by Juno. Geophys. Res. Lett. **44**, 4694–4700 (2017)
M. French, A. Becker, W. Lorenzen, N. Nettelmann, M. Bethkenhagen, J. Wicht, R. Redmer, Ab initio simulations for material properties along the Jupiter adiabat. Astrophys. J. Suppl. **202**(1), 5 (2012)
E. Galanti, Y. Kaspi, An adjoint based method for the inversion of the Juno and Cassini gravity measurements into wind fields. Astrophys. J. **820**, 91 (2016)

E. Galanti, Y. Kaspi, Prediction for the flow-induced gravity field of Saturn: implications for Cassini's Grande Finale. Astrophys. J. Lett. **843**, 25 (2017)
E. Galanti, Y. Kaspi, E. Tziperman, A full, self-consistent, treatment of thermal wind balance on fluid planets. J. Fluid Mech. **810**, 175–195 (2017)
E. Galanti, Y. Kaspi, Y. Miguel, T. Guillot, D. Durante, P. Racioppa, L. Iess, Saturn's deep atmospheric flows revealed by the Cassini grand finale gravity measurements. Geophys. Res. Lett. **46**(2), 616–624 (2019)
E. García-Melendo, S. Pérez-Hoyos, A. Sánchez-Lavega, R. Hueso, Saturn's zonal wind profile in 2004-2009 from Cassini ISS images and its long-term variability. Icarus **215**(1), 62–74 (2011)
T. Gastine, J. Wicht, J.M. Aurnou, Zonal flow regimes in rotating anelastic spherical shells: an application to giant planets. Icarus **225**, 156–172 (2013)
T. Guillot, Y. Miguel, B. Militzer, W.B. Hubbard, Y. Kaspi, E. Galanti, H. Cao, R. Helled, S.M. Wahl, L. Iess, W.M. Folkner, D.J. Stevenson, J.I. Lunine, D.R. Reese, A. Biekman, M. Parisi, D. Durante, J.E.P. Connerney, S.M. Levin, S.J. Bolton, A suppression of differential rotation in Jupiter's deep interior. Nature **555**, 227–230 (2018)
M. Heimpel, J. Aurnou, J. Wicht, Simulation of equatorial and high-latitude jets on Jupiter in a deep convection model. Nature **438**, 193–196 (2005)
M. Heimpel, T. Gastine, J. Wicht, Simulation of deep-seated zonal jets and shallow vortices in gas giant atmospheres. Nat. Geosci. **9**, 19–23 (2016)
I.M. Held, V.D. Larichev, A scaling theory for horizontally homogeneous, baroclinically unstable flow on a beta plane. J. Atmos. Sci. **53**(7), 946–952 (1996)
R. Helled, J.D. Anderson, G. Schubert, Uranus and Neptune: shape and rotation. Icarus **210**, 446–454 (2010)
R. Helled, J.D. Anderson, M. Podolak, G. Schubert, Interior models of Uranus and Neptune. Astrophys. J. **726**, 15 (2011)
R. Helled, E. Galanti, Y. Kaspi, Saturn's fast spin determined from its gravitational field and oblateness. Nature **520**, 202–204 (2015)
H.P. Huang, W.A. Robinson, Two-dimentional turbulence and persistent jets in a global barotropic model. J. Atmos. Sci. **55**, 611–632 (1998)
W.B. Hubbard, Gravitational field of a rotating planet with a polytropic index of unity. Sov. Astron. **18**, 621–624 (1975)
W.B. Hubbard, *Planetary Interiors* (Van Nostrand-Reinhold, New York, 1984), p. 343
W.B. Hubbard, Note: gravitational signature of Jupiter's deep zonal flows. Icarus **137**, 357–359 (1999)
W.B. Hubbard, High-precision Maclaurin-based models of rotating liquid planets. Astrophys. J. Lett. **756**, 15 (2012)
W.B. Hubbard, M.S. Marley, Optimized Jupiter, Saturn, and Uranus interior models. Icarus **78**, 102–118 (1989)
W.B. Hubbard, B. Militzer, A preliminary Jupiter model. Astrophys. J. **820**, 80 (2016)
W.B. Hubbard, W.J. Nellis, A.C. Mitchell, N.C. Holmes, P.C. McCandless, S.S. Limaye, Interior structure of Neptune - comparison with Uranus. Science **253**, 648–651 (1991)
L. Iess, W.M. Folkner, D. Durante, M. Parisi, Y. Kaspi, E. Galanti, T. Guillot, W.B. Hubbard, D.J. Stevenson, J.D. Anderson, D.R. Buccino, L.G. Casajus, A. Milani, R. Park, P. Racioppa, D. Serra, P. Tortora, M. Zannoni, H. Cao, R. Helled, J.I. Lunine, Y. Miguel, B. Militzer, S. Wahl, J.E.P. Connerney, S.M. Levin, S.J. Bolton, Measurement of Jupiter's asymmetric gravity field. Nature **555**, 220–222 (2018)
L. Iess, B. Militzer, Y. Kaspi, P. Nicholson, D. Durante, P. Racioppa, A. Anabtawi, E. Galanti, W.B. Hubbard, M.J. Mariani, P. Tortora, S. Wahl, M. Zannoni, Measurement and implications of Saturn's gravity field and ring mass. Science **364**, 1052 (2019)
R.A. Jacobson, JUP230 orbit solutions (2003). http://ssd.jpl.nasa.gov/
R.A. Jacobson, The gravity field of the Uranian system and the orbits of the Uranian satellites and rings, in *AAS/Division for Planetary Sciences Meeting Abstracts #39*. Bull. Am. Astro. Soc., vol. 38 (2007), p. 453
R.A. Jacobson, The orbits of the Neptunian satellites and the orientation of the pole of Neptune. Astrophys. J. **137**, 4322–4329 (2009)
R.A. Jacobson, P.G. Antreasian, J.J. Bordi, K.E. Criddle, R. Ionasescu, J.B. Jones, R.A. Mackenzie, M.C. Meek, D. Parcher, F.J. Pelletier, W.M. Owen Jr., D.C. Roth, I.M. Roundhill, J.R. Stauch, The gravity field of the Saturnian system from satellite observations and spacecraft tracking data. Astrophys. J. **132**, 2520–2526 (2006)
C.A. Jones, K.M. Kuzanyan, Compressible convection in the deep atmospheres of giant planets. Icarus **204**, 227–238 (2009)
Y. Kaspi, Turbulent Convection in Rotating Anelastic Spheres: a Model for the Circulation on the Giant Planets. PhD thesis, Massachusetts Institute of Technology (2008)
Y. Kaspi, Inferring the depth of the zonal jets on Jupiter and Saturn from odd gravity harmonics. Geophys. Res. Lett. **40**, 676–680 (2013)

Y. Kaspi, G.R. Flierl, Formation of jets by baroclinic instability on gas planet atmospheres. J. Atmos. Sci. **64**, 3177–3194 (2007)
Y. Kaspi, G.R. Flierl, A.P. Showman, The deep wind structure of the giant planets: results from an anelastic general circulation model. Icarus **202**, 525–542 (2009)
Y. Kaspi, W.B. Hubbard, A.P. Showman, G.R. Flierl, Gravitational signature of Jupiter's internal dynamics. Geophys. Res. Lett. **37**, 01204 (2010)
Y. Kaspi, A.P. Showman, W.B. Hubbard, O. Aharonson, R. Helled, Atmospheric confinement of jet-streams on Uranus and Neptune. Nature **497**, 344–347 (2013)
Y. Kaspi, J.E. Davighi, E. Galanti, W.B. Hubbard, The gravitational signature of internal flows in giant planets: comparing the thermal wind approach with barotropic potential-surface methods. Icarus **276**, 170–181 (2016)
Y. Kaspi, E. Galanti, R. Helled, Y. Miguel, W.B. Hubbard, B. Militzer, S. Wahl, S. Levin, J. Connerney, S. Bolton, The effect of differential rotation on Jupiter's low-degree even gravity moments. Geophys. Res. Lett. **44**, 5960–5968 (2017)
Y. Kaspi, E. Galanti, W.B. Hubbard, D.J. Stevenson, S.J. Bolton, L. Iess, T. Guillot, J. Bloxham, J.E.P. Connerney, H. Cao, D. Durante, W.M. Folkner, R. Helled, A.P. Ingersoll, S.M. Levin, J.I. Lunine, Y. Miguel, B. Militzer, M. Parisi, S.M. Wahl, Jupiter's atmospheric jet streams extend thousands of kilometres deep. Nature **555**, 223–226 (2018)
D. Kong, K. Zhang, G. Schubert, A fully self-consistent multi-layered model of Jupiter. Astrophys. J. **826**, 127 (2016a)
D. Kong, K. Zhang, G. Schubert, Odd gravitational harmonics of Jupiter: effects of spherical versus non-spherical geometry and mathematical smoothing of the equatorially antisymmetric zonal winds across the equatorial plane. Icarus **277**, 416–423 (2016b)
D. Kong, K. Zhang, G. Schubert, J.D. Anderson, Origin of Jupiter's cloud-level zonal winds remains a puzzle even after Juno. Proc. Natl. Acad. Sci. USA **115**(34), 8499–8504 (2018)
L. Kulowski, H. Cao, J. Bloxham, Contributions to Jupiter's gravity field from dynamics in the dynamo region. J. Geophys. Res., Planets **125**, 2019–006165 (2020)
S. Lee, Baroclinic multiple jets on a sphere. J. Atmos. Sci. **62**, 2484–2498 (2004)
C. Li, A. Ingersoll, S. Bolton, S. Levin, M. Janssen, S. Atreya, J. Lunine, P. Steffes, S. Brown, T. Guillot, M. Allison, J. Arballo, A. Bellotti, V. Adumitroaie, S. Gulkis, A. Hodges, L. Li, S. Misra, G. Orton, F. Oyafuso, D. Santos-Costa, H. Waite, Z. Zhang, The water abundance in Jupiter's equatorial zone. Nat. Astron. **4**, 609–616 (2020)
Y. Lian, A.P. Showman, Deep jets on gas-giant planets. Icarus **194**, 597–615 (2008)
Y. Lian, A.P. Showman, Generation of equatorial jets by large-scale latent heating on the giant planets. Icarus **207**, 373–393 (2010)
J. Liu, Interaction of magnetic field and flow in the outer shells of giant planets. PhD thesis, California Institute of Technology (2006)
J. Liu, T. Schneider, Mechanisms of jet formation on the giant planets. J. Atmos. Sci. **67**, 3652–3672 (2010)
J. Liu, P.M. Goldreich, D.J. Stevenson, Constraints on deep-seated zonal winds inside Jupiter and Saturn. Icarus **196**, 653–664 (2008)
J. Liu, T. Schneider, Y. Kaspi, Predictions of thermal and gravitational signals of Jupiter's deep zonal winds. Icarus **224**, 114–125 (2013)
J. Liu, T. Schneider, L.N. Fletcher, Constraining the depth of Saturn's zonal winds by measuring thermal and gravitational signals. Icarus **239**, 260–272 (2014)
C. Mankovich, M.S. Marley, J.J. Fortney, N. Movshovitz, Cassini ring seismology as a probe of Saturn's interior. I. rigid rotation. Astrophys. J. **871**, 1 (2019)
J. May, T.D. Carr, M.D. Desch, Decametric radio measurement of Jupiter's rotation period. Icarus **40**, 87–93 (1979)
Y. Miguel, T. Guillot, L. Fayon, Jupiter internal structure: the effect of different equations of state. Astron. Astrophys. **596**, 114 (2016)
B. Militzer, W.B. Hubbard, Ab initio equation of state for hydrogen-helium mixtures with recalibration of the giant-planet mass-radius relation. Astrophys. J. **774**, 148 (2013)
B. Militzer, S. Wahl, W.B. Hubbard, Models of Saturn's interior constructed with accelerated concentric Maclaurin spheroid method. Astrophys. J. **879**, 78 (2019)
K. Moore, R. Yadav, L. Kulowski, H. Cao, J. Bloxham, J.E.P. Connerney, S. Kotsiaros, J. Jorgensen, J. Merayo, D. Stevenson, S.J. Bolton, S.M. Levin, A complex Jovian dynamo from the hemispheric dichotomy of Jupiter's field. Nature **561**, 76–78 (2018)
K.M. Moore, H. Cao, J. Bloxham, D.J. Stevenson, J.E.P. Connerney, S.J. Bolton, Time variation of Jupiter's internal magnetic field consistent with zonal wind advection. Nat. Astron. **3**, 730–735 (2019)

W.J. Nellis, A.C. Mitchell, P.C. McCandless, D.J. Erskine, S.T. Weir, Electronic energy gap of molecular hydrogen from electrical conductivity measurements at high shock pressures. Phys. Rev. Lett. **68**(19), 2937–2940 (1992)

N. Nettelmann, A. Becker, B. Holst, R. Redmer, Jupiter models with improved ab initio hydrogen equation of state (H-REOS.2). Astrophys. J. **750**, 52 (2012)

N. Nettelmann, R. Helled, J.J. Fortney, R. Redmer, New indication for a dichotomy in the interior structure of Uranus and Neptune from the application of modified shape and rotation data. Planet. Space Sci. **77**, 143–151 (2013)

R.L. Panetta, Zonal jets in wide baroclinically unstable regions: persistence and scale selection. J. Atmos. Sci. **50**(14), 2073–2106 (1993)

J.C. Pearl, B.J. Conrath, The albedo, effective temperature, and energy balance of Neptune, as determined from Voyager data. J. Geophys. Res. **96**(15), 18921–18930 (1991)

J.C. Pearl, B.J. Conrath, R.A. Hanel, J.A. Pirraglia, The albedo, effective temperature, and energy balance of Uranus, as determined from Voyager iris data. Icarus **84**, 12–28 (1990)

J. Pedlosky, *Geophysical Fluid Dynamics* (Springer, Berlin, 1987), p. 710

P.L. Read, T.E. Dowling, G. Schubert, Saturn's rotation period from its atmospheric planetary-wave configuration. Nature **460**, 608–610 (2009)

P.B. Rhines, Waves and turbulence on a beta plane. J. Fluid Mech. **69**, 417–443 (1975)

A.C. Riddle, J.W. Warwick, Redefinition of System III longitude. Icarus **27**, 457–459 (1976)

C. Salyk, A.P. Ingersoll, J. Lorre, A. Vasavada, A.D. Del Genio, Interaction between eddies and mean flow in Jupiter's atmosphere: analysis of Cassini imaging data. Icarus **185**, 430–442 (2006)

A. Sánchez-Lavega, T. del Río-Gaztelurrutia, R. Hueso, J.M. Gómez-Forrellad, J.F. Sanz-Requena, J. Legarreta, E. García-Melendo, F. Colas, J. Lecacheux, L.N. Fletcher, D. Barrado y Navascués, D. Parker, T. Akutsu, T. Barry, J. Beltran, S. Buda, B. Combs, F. Carvalho, P. Casquinha, M. Delcroix, S. Ghomizadeh, C. Go, J. Hotershall, T. Ikemura, G. Jolly, A. Kazemoto, T. Kumamori, M. Lecompte, P. Maxson, F.J. Melillo, D.P. Milika, E. Morales, D. Peach, J. Phillips, J.J. Poupeau, J. Sussenbach, G. Walker, S. Walker, T. Tranter, A. Wesley, T. Wilson, K. Yunoki (International Outer Planet Watch Team), Deep winds beneath Saturn's upper clouds from a seasonal long-lived planetary-scale storm. Nature **475**(7354), 71–74 (2011)

A. Sánchez-Lavega, L.A. Sromovsky, A.P. Showman, A.D. Del Genio, R.M. Young, R. Hueso, E. Garcia-Melenso, Y. Kaspi, G.S. Orton, N. Barrado-Izagirre, D.S. Choi, J.M. Barbara, in *Zonal Jets: Phenomenology, Genesis, and Physics*, 1st edn., ed. by G. Galperin P. Read (Cambridge University Press, Cambridge, 2019), pp. 72–103. Chap. 4

K.M. Sayanagi, A.P. Showman, T.E. Dowling, The emergence of multiple robust zonal jets from freely evolving, three-dimensional stratified geostrophic turbulence with applications to Jupiter. J. Atmos. Sci. **65**, 3947 (2008)

T. Schneider, J. Liu, Formation of jets and equatorial superrotation on Jupiter. J. Atmos. Sci. **66**, 579–601 (2009)

R.K. Scott, L.M. Polvani, Forced-dissipative shallow-water turbulence on the sphere and the atmospheric circulation of the giant planets. J. Atmos. Sci. **64**, 3158–3176 (2007)

R.K. Scott, L.M. Polvani, Equatorial superrotation in shallow atmospheres. Geophys. Res. Lett. **35**, 24202 (2008)

A.P. Showman, Numerical simulations of forced shallow-water turbulence: effects of moist convection on the large-scale circulation of Jupiter and Saturn. J. Atmos. Sci. **64**, 3132–3157 (2007)

A.P. Showman, P.J. Gierasch, Y. Lian, Deep zonal winds can result from shallow driving in a giant-planet atmosphere. Icarus **182**, 513–526 (2006)

A.P. Showman, R. Achterberg, A.P. Ingersoll, Y. Kaspi, Saturn in the 21st century, in *The Global Atmospheric Circulation of Saturn*, ed. by K. Baines, M. Flasar (Cambridge University Press, Cambridge, 2018)

A.P. Showman, X. Tan, X. Zhang, Atmospheric circulation of brown dwarfs and Jupiter- and Saturn-like planets: zonal jets, long-term variability, and QBO-type oscillations. Astrophys. J. **883**(1), 4 (2019)

A.A. Simon-Miller, B.J. Conrath, P.J. Gierasch, G.S. Orton, R.K. Achterberg, F.M. Flasar, B.M. Fisher, Jupiter's atmospheric temperatures: from Voyager IRIS to Cassini CIRS. Icarus **180**(1), 98–112 (2006)

K.S. Smith, A local model for planetary atmospheres forced by small-scale convection. J. Atmos. Sci. **61**, 1420–1433 (2004)

B.A. Smith, L.A. Soderblom, R. Beebe, D. Bliss, R.H. Brown, S.A. Collins, J.M. Boyce, G.A. Briggs, A. Brahic, J.N. Cuzzi, D. Morrison, Voyager 2 in the Uranian system - imaging science results. Science **233**, 43–64 (1986)

B.A. Smith, L.A. Soderblom, D. Banfield, C. Barnet, R.F. Beebe, A.T. Bazilevskii, K. Bollinger, J.M. Boyce, G.A. Briggs, A. Brahic, Voyager 2 at Neptune - imaging science results. Science **246**, 1422–1449 (1989)

A. Spiga, S. Guerlet, E. Millour, M. Indurain, Y. Meurdesoif, S. Cabanes, T. Dubos, J. Leconte, A. Boissinot, S. Lebonnois, M. Sylvestre, T. Fouchet, Global climate modeling of Saturn's atmosphere. Part II: Multi-annual high-resolution dynamical simulations. Icarus **335**, 113377 (2020)
D.J. Stevenson, Planetary magnetic fields. Earth Planet. Sci. Lett. **208**(1–2), 1–11 (2003)
D.J. Stevenson, Jupiter's interior as revealed by Juno. Annu. Rev. Earth Planet. Sci. **48**, 465–489 (2020)
D.J. Stevenson, E.E. Salpeter, The phase diagram and transport properties for hydrogen-helium fluid planets. Astrophys. J. Suppl. **35**, 221–237 (1977)
A. Studwell, L. Li, X. Jiang, K.H. Baines, P.M. Fry, T.W. Momary, U.A. Dyudina, Saturn's global zonal winds explored by Cassini/VIMS 5-μm images. Geophys. Res. Lett. **45**, 6823–6831 (2018)
Z.-P. Sun, G. Schubert, G.A. Glatzmaier, Banded surface flow maintained by convection in a model of the rapidly rotating giant planets. Science **260**, 661–664 (1993)
J. Tollefson, M.H. Wong, I. de Pater, A.A. Simon, G.S. Orton, J.H. Rogers, S.K. Atreya, R.G. Cosentino, W. Januszewski, R. Morales-Juberías, P.S. Marcusi, Changes in Jupiter's zonal wind profile preceding and during the Juno mission. Icarus **296**, 163–178 (2017)
G.K. Vallis, *Atmospheric and Oceanic Fluid Dynamics: Fundamentals and Large-Scale Circulation*, 2nd edn. (Cambridge University Press, Cambridge, 2017), p. 946
G.K. Vallis, M.E. Maltrud, Generation of mean flows and jets on a beta plane and over topography. J. Phys. Oceanogr. **23**, 1346–1362 (1993)
A.R. Vasavada, A.P. Showman, Jovian atmospheric dynamics: an update after Galileo and Cassini. Rep. Prog. Phys. **68**, 1935–1996 (2005)
S. Wahl, W.B. Hubbard, B. Militzer, N.M.Y. Movshovitz, Y. Kaspi, R. Helled, D. Reese, E. Galanti, S. Levin, J. Connerney, S. Bolton, Comparing Jupiter interior structure models to Juno gravity measurements and the role of an expanded core. Geophys. Res. Lett. **44**, 4649–4659 (2017)
E.S. Warneford, P.J. Dellar, Thermal shallow water models of geostrophic turbulence in Jovian atmospheres. Phys. Fluids **26**(1), 016603 (2014)
J. Wicht, C.A. Jones, K. Zhang, Instability of zonal flows in rotating spherical shells: an application to Jupiter. Icarus **155**, 425–435 (2002)
J. Wicht, T. Gastine, L.D.V. Duarte, Dynamo action in the steeply decaying conductivity region of Jupiter-like dynamo models. J. Geophys. Res., Planets **124**(3), 837–863 (2019)
J. Wicht, W. Dietrich, P. Wulff, U.R. Christensen, Linking zonal winds and gravity: the relative importance of dynamic self gravity. Mon. Not. R. Astron. Soc. **492**, 3364–3374 (2020)
G.P. Williams, Planetary circulations: Part I: Barotropic representation of the Jovian and terrestrial turbulence. J. Atmos. Sci. **35**, 1399–1426 (1978)
G.P. Williams, Planetary circulations. Part II: The Jovian quasi-geostrophic regime. J. Atmos. Sci. **36**, 932–968 (1979)
R.M.B. Young, P.L. Read, Y. Wang, Simulating Jupiter's weather layer. Part I: Jet spin-up in a dry atmosphere. Icarus **326**, 225–252 (2019)
K. Zhang, D. Kong, G. Schubert, Thermal-gravitational wind equation for the wind-induced gravitational signature of giant gaseous planets: mathematical derivation, numerical method and illustrative solutions. Astrophys. J. **806**, 270–279 (2015)